Klimkowski, Ł., Nagy, S., Papiernik, B., Orlic, B., Kempka, T. (2015): Numerical Simulations of Enhanced Gas Recovery at the Załęcze Gas Field in Poland Confirm High CO 2 Storage Capacity and Mechanical Integrity. - *Oil & Gas Science and Technology*, *70*, 4, p. 655-680.

DOI: http://doi.org/10.2516/ogst/2015012

Oil & Gas Science and Technology – Rev. IFP Energies nouvelles, Vol. 70 (2015), No. 4, pp. 655-680

DOI: 10.2516/ogst/2015012

Dossier

Characterization of European CO_2 Storage – European Project SiteChar
Caractérisation de sites européens de stockage de CO_2 – Projet européen SiteChar

Numerical Simulations of Enhanced Gas Recovery at the Załęcze Gas Field in Poland Confirm High CO_2 Storage Capacity and Mechanical Integrity

Łukasz Klimkowski[1], Stanisław Nagy[1], Bartosz Papiernik[1], Bogdan Orlic[2] and Thomas Kempka[3]*

[1] *AGH University of Science & Technology, Aleja Adama Mickiewicza 30, 30-059 Kraków - Poland*
[2] *TNO, Earth, Environmental and Life Sciences, Princetonlaan 6, NL-3584 CB Utrecht - The Netherlands*
[3] *GFZ German Research Centre for Geosciences, Telegrafenberg, 14473 Potsdam - Germany*
e-mail: kempka@gfz-potsdam.de

* Corresponding author

Abstract — *Natural gas from the Załęcze gas field located in the Fore-Sudetic Monocline of the Southern Permian Basin has been produced since November 1973, and continuous gas production led to a decrease in the initial reservoir pressure from 151 bar to about 22 bar until 2010. We investigated a prospective enhanced gas recovery operation at the Załęcze gas field by coupled numerical hydro-mechanical simulations to account for the CO_2 storage capacity, trapping efficiency and mechanical integrity of the reservoir, caprock and regional faults. Dynamic flow simulations carried out indicate a CO_2 storage capacity of 106.6 Mt with a trapping efficiency of about 43% (45.8 Mt CO_2) established after 500 years of simulation. Two independent strategies on the assessment of mechanical integrity were followed by two different modeling groups resulting in the implementation of field- to regional-scale hydro-mechanical simulation models. The simulation results based on application of different constitutive laws for the lithological units show deviations of 31% to 93% for the calculated maximum vertical displacements at the reservoir top. Nevertheless, results of both simulation strategies indicate that fault reactivation generating potential leakage pathways from the reservoir to shallower units is very unlikely due to the low fault slip tendency (close to zero) in the Zechstein caprocks. Consequently, our simulation results also emphasise that the supra- and subsaliniferous fault systems at the Załęcze gas field are independent and very likely not hydraulically connected. Based on our simulation results derived from two independent modeling strategies with similar simulation results on fault and caprock integrity, we conclude that the investigated enhanced gas recovery scheme is feasible, with a negligibly low risk of relevant fault reactivation or formation fluid leakage through the Zechstein caprocks.*

Résumé — **Des simulations numériques de récupération assistée de gaz sur un gisement de gaz de Załęcze en Pologne confirment les capacités de stockage de CO_2 élevées et l'intégrité mécanique dudit gisement** — Le gaz naturel du gisement de Załęcze, situé dans la structure monoclinale de la région des Sudètes au niveau du Bassin Permien sud, est produit depuis novembre 1973, moyennant quoi la production de gaz continue a donné lieu à une diminution de la pression initiale du réservoir de 151 bar à environ 22 bar en 2010. Nous avons effectué une étude prospective mettant en jeu une opération de récupération de gaz améliorée sur le gisement de gaz de Załęcze par des simulations

hydromécaniques numériques couplées et prenant en compte les capacités de stockage de CO_2, l'efficacité de piégeage et l'intégrité mécanique du gisement, des roches couverture et des failles régionales. Les simulations hydrodynamiques réalisées indiquent une capacité de stockage de CO_2 de 106,6 Mt avec une efficacité de piégeage d'environ 43 % (45,8 Mt de CO_2) établie après 500 ans de simulation. Deux stratégies indépendantes pour l'évaluation de l'intégrité mécanique ont été suivies par deux équipes différentes donnant lieu à la mise en œuvre de modèles de simulation hydromécaniques de l'échelle du gisement jusqu'à l'échelle régionale. Les résultats de simulation basés sur l'application de différentes lois constitutives pour les unités lithologiques présentent des écarts de 31 % à 93 % pour les déplacements verticaux maximum calculés au niveau supérieur du réservoir. Toutefois, les deux stratégies de simulation montrent qu'une réactivation des failles susceptible de générer des voies de fuite potentielles du réservoir vers des unités moins profondes, est improbable du fait de la tendance à un faible glissement de faille dans les roches couvertures de Zechstein. Nos résultats de simulation soulignent également que les systèmes de failles supra- et sous-salinifères du gisement gazier de Załęcze sont indépendants et vraisemblablement pas reliés hydrauliquement. Sur la base des simulations associées aux deux stratégies de modélisation indépendantes, et qui présentent des résultats similaires en matière d'intégrité des roches couverture et des failles, nous concluons que le schéma de récupération assistée de gaz étudié est réalisable, avec un risque négligeable de réactivation de la faille ou de fuite du fluide de formation à travers les roches couverture du Zechstein.

INTRODUCTION

Enhanced Gas Recovery (EGR) from depleted natural gas fields by CO_2 injection is considered as an economic option for greenhouse gas emission mitigation and as an efficient way to maintain gas production from low-pressure gas reservoirs (Kühn *et al*., 2012, 2013; Hussen *et al*., 2012; Polak and Grimstad, 2009; Oldenburg *et al*., 2004). Production from the Załęcze natural gas field located in the Fore-Sudetic Monocline of the Southern Permian Basin has been undertaken since November 1973. In this context, the initial reservoir pressure of 151 bar was decreased by about 130 bar until 2011, indicating significant CO_2 storage capacity that may be also derived from the natural gas volume of 19.25 billion sm^3 produced from the reservoir until the end of 2010. The aim of the present study is the assessment of the CO_2 storage capacity and trapping efficiency in addition to a detailed investigation of hydro-mechanical effects resulting from 40 years of gas production followed by an EGR operation thereafter. An assessment of hydro-mechanical effects allows defining the constraints required for a safe EGR operation not posing a risk to the mechanical integrity of the reservoir, its caprocks and adjacent geological faults (Rutqvist, 2012; Hawkes *et al*., 2004). Coupled hydro-mechanical simulations on CO_2 storage without any natural gas production have been carried out in different contexts (Kempka *et al*., 2015; Tillner *et al*., 2014; Magri *et al*., 2013; Orlic and Wassing, 2013; Röhmann *et al*., 2013; Vidal-Gilbert *et al*., 2009). However, only simplified hydro-mechanical numerical simulation models, *e.g.* for benchmarking purposes, have been published on EGR operations (Gou *et al*., 2014; Hou *et al*., 2012). As the complex geology in the Załęcze natural gas field requires more sophisticated numerical models to be employed, we implemented coupling strategies using complex hydro-mechanical models with numerous geological faults from the reservoir up to the regional scale in order to account for vertical displacements as well as reservoir, caprock and fault integrity. The hydro-mechanical simulation results can be employed for quantification of potential CO_2 and/or formation fluid leakage *via* faults, as recently discussed by Jamaloei (2013), Tillner *et al*. (2013), Pruess (2011), Cappa and Rutqvist (2011).

1 ZAŁĘCZE NATURAL GAS FIELD

The geology of the Załęcze gas reservoir as well as the static model development process are discussed in detail by Papiernik *et al*. (2012). In the following, only a short summary of the most important aspects related to the regional geology is addressed. The Załęcze and Żuchlów gas fields are located in South-Western Poland, in the Fore-Sudetic Monocline within the Silesian Sedimentary Basin (Fig. 1), which is a marginal part of the Southern Permian Basin (SPB). Sandstones accumulated in the Upper Rotliegend and the overlaying Zechstein Limestone (Ca1) form the reservoir of the Carboniferous Total Petroleum System (CTPS) (Magoon and Schmoker, 2000), which is one of the most important European petroleum provinces (Karnkowski, 2007; Pletsch *et al*., 2010). The basal and marginal parts

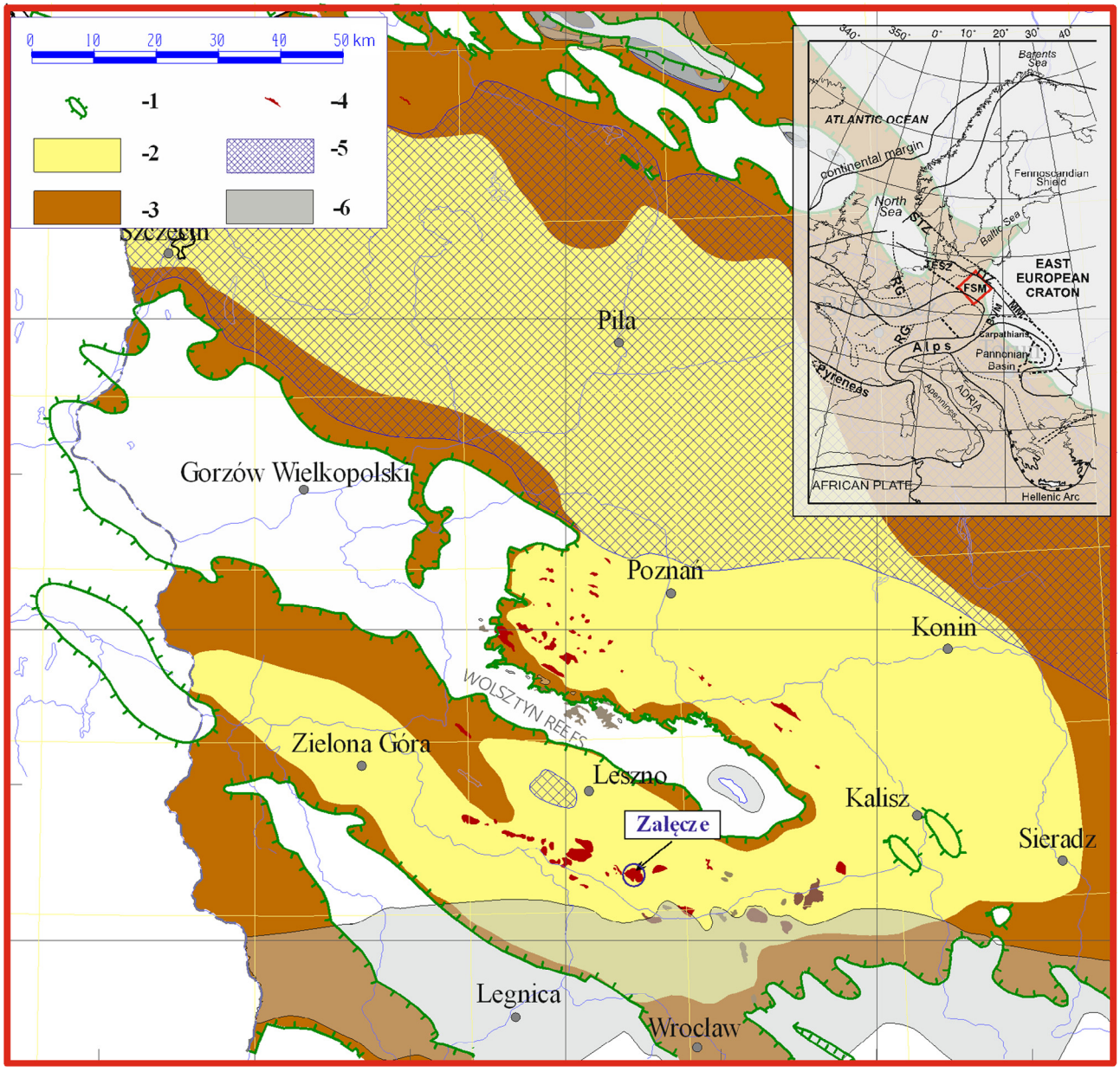

Figure 1

Area map of Rotliegend and Zechstein Limestone (Ca1 Carbonate) reservoirs as well as reservoir facies distribution. 1 - Extent of Rotliegend deposits; 2 - Aeolian facies (R); 3 - Fluvial facies (R); 4 - Gas fields; 5 - Non-reservoir playa; 6 - Carbonate platforms and reefs of Ca1, modified after Jarzyna *et al.* (2009).

of the Silesian Basin are dominated by fluvial sandstones with aeolian intercalations. The upper part of the Rotliegend profile and the axial zone of the Silesian Basin Rotliegend are represented by aeolian deposits. The width of the Upper Rotliegend (Saxonian) deposits subcrops in the Silesian Basin up to 60 km, while their thickness ranges up to about 400 m in the axial part. The thickness of the Zechstein limestone (Ca1) is up to 60 m (Papiernik *et al.*, 2008), while the Rotliegend thickness in the Załęcze-Żuchlów study area is between 50 m and 400 m, with the Ca1 Carbonate reservoir thickness not exceeding 15 m (Tab. 1).

The Rotliegend reservoir in the Załęcze-Żuchlów area is effectively sealed by the caprock consisting of Zechstein deposits located above the Basal Limestone (Ca1).

TABLE 1

Stratigraphic column of the Fore-Sudetic Monocline in the Załęcze-Żuchlów area. Reservoirs discussed in the present study are printed in bold letters

Quaternary	Q		Gravels, sands, clays
Tertiary	Tr		Shales, clays, muds
Middle Triassic	Tm - Muschelkalk		Carbonates, marls, shales
Lower Triassic	Tp3 - Upper Buntsandstein (Ret)		Carbonates, marls, shales
	Tp2 - Middle Buntsandstein		Sandstones. mudstones, shales
	Tp1 - Lower Buntsandstein		Sandstones. mudstones, shales
Upper Permian	Rewala Formation PZ4d + PZ4e	Terrigenic formation	Mud-, clay-, sandstones
	PZ4C	Top youngest halite	Halite
	PZ4b	Upper red pelite (upper part)	Claystones
		Intrastratal halite	Intrastratal halites
		Upper red pelite (lower part)	Claystones
	PZ4a	Upper youngest clay Halite	Claystones, halite
		Upper pegmatite ahydrite	Anhydrite
		Lower pegmatite anhydrite	Anhydrite
		Lower red pelite	Claystones
	PZ3	Younger halite	Halite
		Main anhydrite	Anhydrite
		Platy dolomite	Dolomite
		Grey pelite	Claystones
	PZ2	Screening anhydrite	Anhydrite
		Screening older halite	Halite
		Older potash (older halite)	Potash salt, halite
		Basal anhydrite	Anhydrite
		Main dolomite	**Dolomite, carbonates (Ca2)**
	PZ1	Upper anhydrite	Anhydrite
		Oldest halite	Halite
		Lower anhydrite	Anhydrite
		Zechstein Limestone	**Zechstein Limestone (Ca1 Carbonate reservoir)**
Lower Permian	Upper Rotliegend		**Aeolian and fluvial sandstones (Saxonian reservoir)**
	Lower Rotliegend (Autunian)		Fluvial, aluvial sandstones and mudstones, volcanic rocks
Carboniferous	Variscian Orogen		Mudstones, shales, sandstones

The direct seal of the CTPS consists of anhydrites and salts of the PZ1 Cyclotheme. These anhydrites are superimposed by the Main Dolomite Carbonates of the PZ2 Cyclotheme representing gas- and oil-bearing deposits acting as source rocks and reservoirs of the Zechstein Petroleum System (Pletsch *et al.*, 2010; Karnkowski, 1999). Within the area of the Fore-Sudetic Monocline, the Ca2 Carbonate reservoir can be treated as a secondary reservoir for CO_2 storage. Its caprock constitutes anhydrites, salts and shales (Papiernik *et al.*, 2012).

The Załęcze-Żuchlów reservoir structure was identified in the mid-1960s by seismic exploration and the first appraisal wells were drilled and tested in the early 1970s; the field closure area has been delineated by more than 50 appraisal and development wells. The crest of the structure is at 1 232 metres below sea level (m.b.s.l.) and the gas-water contact at 1 354 m. The average reservoir porosity is about 18.5% and permeability ranges between 5 mD and 50 mD . The Rotliegend reservoir is underlain by an aquifer, but production performance suggests that this aquifer is inactive as most of the down-dip wells produce dry gas. The underlying Carboniferous basement has not yet been penetrated by any wells. Gas production started in November 1973 indicating a high nitrogen content (25% by mole), but a complete lack of hydrogen sulphide. A total of 49 production wells have been drilled, among which 36 were still producing gas in March 2011. The initial reservoir pressure was 151 bar and reduced to about 22 bar in 2011 due to extensive natural gas production. In 2010, 181 million sm^3 of natural gas were produced, while the cumulative production from the Załęcze gas field amounted to 19.25 billion sm^3 at the end of the year.

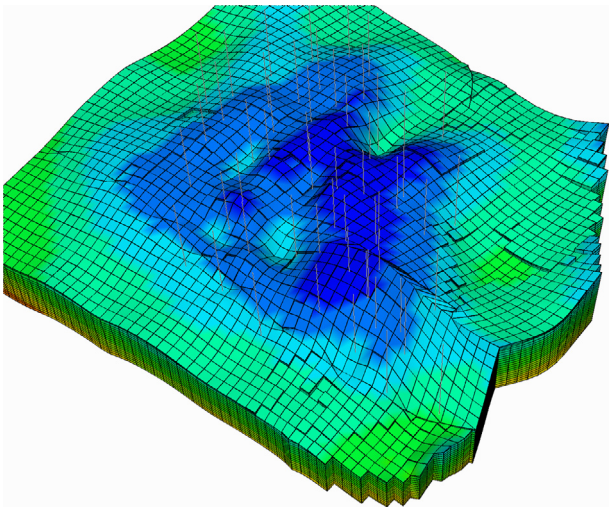

Figure 2

3D view of the Załęcze reservoir model used for dynamic flow simulations with an areal extent of 8.6 km × 8.0 km. North is in the normal direction of the lower border.

2 DYNAMIC FLOW SIMULATIONS OF CO_2 INJECTION

2.1 Methodology and Model Implementation

A static model was constructed using the Petrel E&P software platform (Schlumberger, 2012) within two major steps. First, a detailed regional model of the Rotliegend reservoirs and their overburden was elaborated for the entire Załęcze-Żuchlów area. Then, local upscaling of the reservoir sections was performed, allowing for extracting and refining the local reservoir models of the Załęcze and Żuchlów gas fields. The last step in the static modeling process was the model export in the RESCUE exchange standard format to allow data transfer from the Petrel software to the CMG simulation package (CMG, 2011), which was then applied for the dynamic flow simulations. The reservoir model was attributed with porosity, permeability and net to gross ratio information.

The static model is discretised by 118 × 124 × 62 elements exceeding the Załęcze reservoir area laterally and including the overburden layers to account for pore pressure perturbation in the first caprock above the reservoir. The dynamic simulation model is based on the static model, but only consisting of two horizons: the basal Zechstein carbonates (Ca1) and the main Saxonian aeolian upper Rotliegend deposits dominated by aeolian sandstones constituting the reservoir rock. A 3D view of the dynamic flow simulation model is plotted in Figure 2.

The composition of the natural gas from the Załęcze field is determined by 13 main components: nine hydrocarbons and four non-hydrocarbons (Tab. 2). In order to make long-term compositional simulations of the reservoir computationally feasible, the number of components in the PVT model was reduced to six (Tab. 3). The lumping procedure carried out had to ensure that the reservoir fluids are represented with an accuracy high enough to account for all compositional effects expected to occur in the reservoir. An internal algorithm of the CMG simulator was used to reduce the number of components in the fluid PVT model by merging components with similar basic thermodynamic parameters into pseudo-components and estimation of their average properties. This procedure resulted in six pseudo-components in addition to the CO_2 that were incorporated into the dynamic flow simulation model.

The Załęcze reservoir has now been operated for more than 40 years. During this time, only minor water production was observed, allowing the reservoir to be treated as a volumetric system, which is also supported by the history matching simulation results. Hence, no-flow conditions were

assumed at the model boundaries, and in order to account for a hydro-mechanical worst case in the coupled hydro-mechanical simulations discussed in Section 3, faults cutting the Załęcze reservoir were integrated as hydraulically sealing faults into the dynamic flow simulation model. Since CO_2 is injected below the gas-water contact, the underlying aquifer was modeled numerically to its bottom. The dynamic flow model was initialised with a reservoir pressure of 151 bar and a constant temperature of 45°C. Based on extensive well log data, the gas and water contact depth was set to 1 354 m below sea level, resulting in 21.81 billion sm^3 of original gas in place.

TABLE 2
Initial natural gas composition in the Załęcze reservoir

Component	Composition (% by mole)
CH_4	73.8453
C_2H_6	0.7962
C_3H_8	0.0748
i-C_4H_{10}	0.0077
n-C_4H_{10}	0.0125
i-C_5H_{12}	0.0038
n-C_5H_{12}	0.0049
C_6H_{14}	0.0046
C7+	0.0038
N_2	24.8384
CO_2	0.2452
H_2	0.0025
He	0.1603

TABLE 3
Gas composition following the lumping procedure and applied in the dynamic flow simulations

Hypothetical components	Composition (% by mole)	Molecular weight (g/mole)
1	0.988490	19.058
2	0.010415	33.352
3	0.000748	44.097
4	0.000202	58.124
5	0.000061	72.151
6	0.000084	90.524

2.2 History Matching and CO_2 Injection Regime

Production data available for the Załęcze gas field consist of monthly gas and water production rates for each of the 40 production wells as well as periodic (on a yearly basis) well bottomhole pressure measurements from 1973 to 2010. These data were used for model calibration in the scope of the history-matching process by introducing the gas production rates as a main constraint and the well bottomhole pressures as well as water production rates as matching parameters. During the history-matching process, static model parameters such as porosity and net to gross ratio were adapted within the range of input data uncertainty. Relative permeability curves were adjusted during the process, with the resulting curves plotted in Figure 3.

An injection rate of 0.9 Mt CO_2/year was applied as determined from the point of view of regional Polish industrial needs. Hereby, the maximum bottomhole pressure for the CO_2 injection wells was limited to 150 bar. The first scenario covers continuous injection for a period of 20 years followed by a monitoring period of 500 years. CO_2 injection is performed simultaneously with natural gas production; production wells are shut in when one of the prescribed constraints, namely the minimum gas production rate (1 440 sm^3/day) and/or bottomhole pressure (10 bar) and/or maximum CO_2 mole fraction in the produced gas (10% by mole) is achieved. These constraints were determined in order to meet the production requirements of an EGR operation at the Załęcze gas field.

The aim of the second simulation scenario was to investigate the dynamic CO_2 storage capacity in the Załęcze reservoir. Identical conditions were applied here except for the duration of the injection period, which was only limited by the

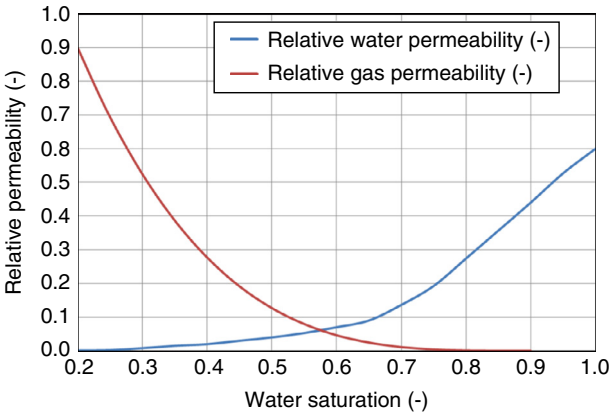

Figure 3
Relative permeability curves applied in the dynamic flow simulation model.

maximum bottomhole pressure of 151 bar (initial reservoir pressure). The CO_2 trapping efficiency is analysed by using trapping efficiency indices, as defined by Nghiem *et al.* (2010):

$$\textit{Residual gas Trapping Index } RTI(t) = \frac{\textit{Total mass of } CO_2 \textit{ trapped as residual gas at time } t}{\textit{Total mass of } CO_2 \textit{ injected at time } t} \quad (1)$$

$$\textit{Solubility Trapping Index } STI(t) = \frac{\textit{Total mass of } CO_2 \textit{ soluble in brine at time } t}{\textit{Total mass of } CO_2 \textit{ injected at time } t} \quad (2)$$

$$\textit{Trapping Efficiency Index } TEI(t) = RTI(t) + STI(t) \quad (3)$$

Two wells located at the eastern contour of the Załęcze gas field were selected for CO_2 injection. Załęcze-3 is located close to the reservoir contour and was not used for gas production, while Załęcze-8 was one of the producing wells and applied for injection in the present study. Both injection wells are perforated below the gas-water contact depth (Załęcze-3 at a depth interval of 1 446 m to 1 476 m and Załęcze-8 at a depth interval of 1 427 m to 1 457 m). Hence, the chosen injection scheme delays upward CO_2 migration and increases its spatial and time-dependent contact with the formation fluid. Thus, CO_2 dissolution can be significantly enhanced, increasing the total trapping efficiency.

2.3 Simulation Results and Discussion

During 20 years of simulated continuous injection, a total amount of about 17.8 Mt CO_2 is stored in the Załęcze reservoir. This leads to an increase in the average reservoir pressure to 39.5 bar (26% of the initial reservoir pressure) at the end of injection and induces a slight increase for the next few decades until a maximum pressure of 47.5 bar at about 70 years after the injection stop is reached (Fig. 4). During this period, CO_2 is still migrating from the injection to the gas-water contact depth. At the same time, water imbibition occurs at the former locations of high gaseous CO_2 concentrations, increasing both CO_2 dissolution and residual trapping. From then on, the reservoir pressure starts to decrease very slowly to 46.6 bar until 500 years after the injection stop. Figure 5 presents the change in CO_2 dissolved in brine and residually trapped due to relative permeability hysteresis effects during water imbibition as a fraction of the total injected CO_2. When CO_2 injection starts, almost all CO_2 goes into solution followed by a decrease in the index (STI) as the local maximum dissolved CO_2 saturation in the formation fluid is reached (Fig. 5).

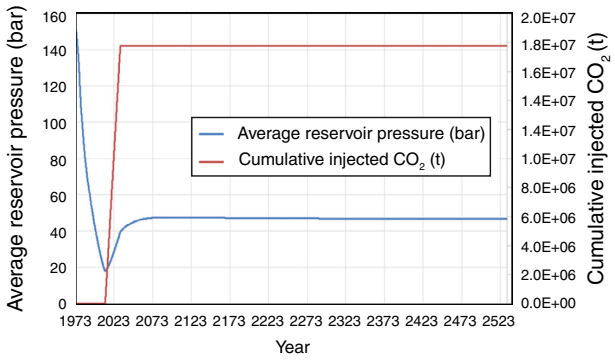

Figure 4

Average reservoir pressure and injected CO_2 mass in the Załęcze reservoir in the first simulation scenario.

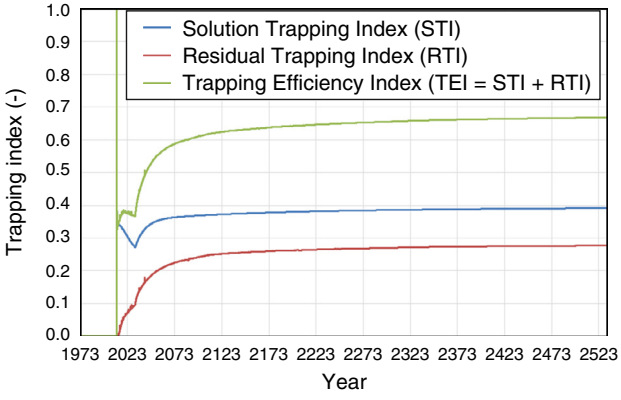

Figure 5

Changes in the solution (STI), residual (RTI) and total (TEI) trapping efficiency indices during the CO_2 injection and post-injection periods in the first simulation scenario.

At the end of the injection operation, 27.1% of the injected CO_2 is dissolved in the formation fluid, increasing to 39.1% in the next 500 years, while the dissolution rate diminishes with time. During the same period, residually trapped CO_2 increases from 9.6% to 27.8%. Total trapping efficiency is 66.9%, with a total trapped CO_2 mass of about 11.9 Mt. CO_2 behaviour at the early stage of injection is presented in Figure 6. CO_2 injected below the gas-water contact arrives at the gas cap after almost two years of injection. Further development and migration of the CO_2 plume is plotted in the combined 3D cross-sections for selected time steps in Figure 7. Even after hundreds of years, a significant amount of CO_2 remains within the reservoir below the gas cap as a result of the relatively high total trapping efficiency.

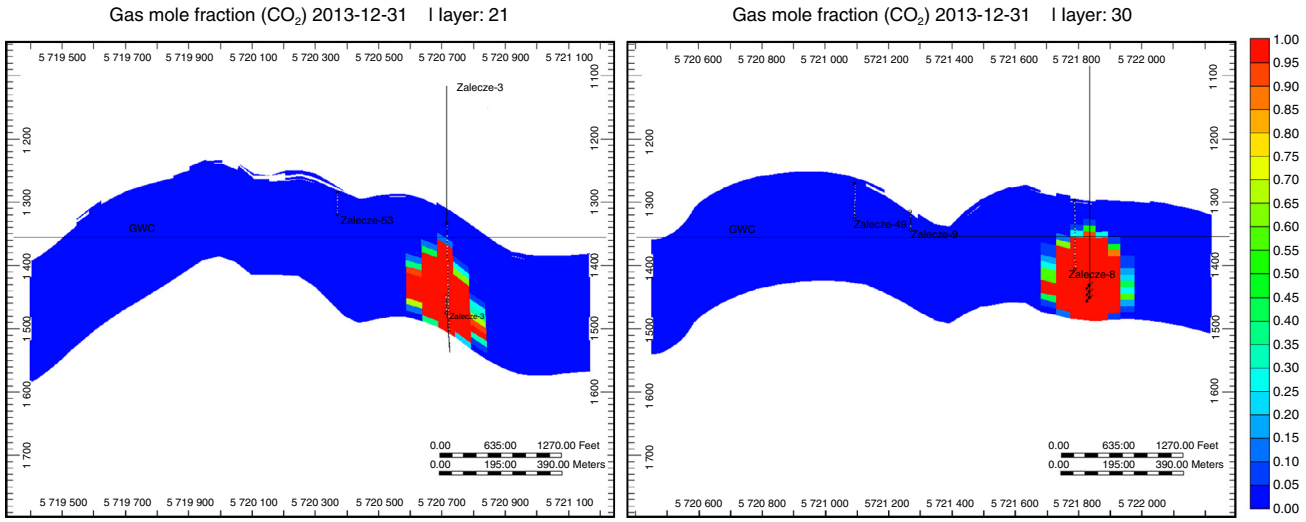

Figure 6

CO_2 mole fraction in cross-sections at both injection wells after two years of injection in the first simulation scenario.

The aim of the second simulation scenario was to assess the maximum storage capacity in the Załęcze reservoir. Figure 8 shows the results of the dynamic storage capacity assessment for the Załęcze reservoir. The initial reservoir pressure of 151 bar is reached after about 118 years of CO_2 injection, while the total injected CO_2 mass amounts to 106.6 Mt. The dynamics of the trapping mechanisms are plotted in Figure 9, indicating that the residual trapping efficiency in both scenarios is almost equal, while CO_2 dissolution is significantly lower in the second simulation scenario due to a higher CO_2 saturation, and hence limitation of CO_2 dissolution by its maximum solubility in the formation fluid. The total trapping efficiency in the second simulation scenario reaches up to 43% after 500 years of simulation. This can be explained, since more than five times the amount of CO_2 was injected into the reservoir in the second scenario, so that residual and solubility trapping are limited by the displacement of the formation fluids and occurrence of a maximum CO_2 saturation at the CO_2-brine contact minimising further CO_2 dissolution.

3 COUPLED HYDRO-MECHANICAL SIMULATIONS

Two different numerical modeling groups carried out an assessment on the reservoir, fault and caprock integrity using their own literature and data interpretation as well as model implementation strategies to ensure an independent review of the mechanical integrity at the Załęcze site. At the time the first (field-scale) strategy was carried out, spatial pore pressure distribution was only available as point data from a few production wells. Consequently, the aim of this simulation strategy was mainly dedicated to an investigation of the impact of elastic *versus* viscoelastic constitutive laws applied for the Zechstein caprock units as well as the effect of hydraulically sealing and non-sealing faults on overall fault integrity in addition to an assessment of vertical displacements. Regional-scale hydro-mechanical simulations carried out thereafter enabled us to integrate the history-matched spatial pore pressure distribution presented in the second dynamic flow simulation scenario. The aim of these simulations was the assessment of the reservoir, caprock and fault integrity considering all 31 major faults mapped in the model domain by Papiernik *et al.* (2012), including the calculation of vertical displacements at the reservoir top and ground surface.

3.1 Field-Scale Hydro-Mechanical Simulation Strategy

Numerical simulations conducted on a field-scale model of the Załęcze reservoir were carried out to assess the hydro-mechanical effects associated with 30 years of gas production followed by 10 years of CO_2 injection. The same field-scale geomechanical model of the Załęcze reservoir was used previously for preliminary assessment of the geomechanical effects, assuming a purely elastic response of all lithological units (Orlic *et al.*, 2013). Here, we extend the previous work by taking into account the time-dependent process of creep in the Zechstein caprock.

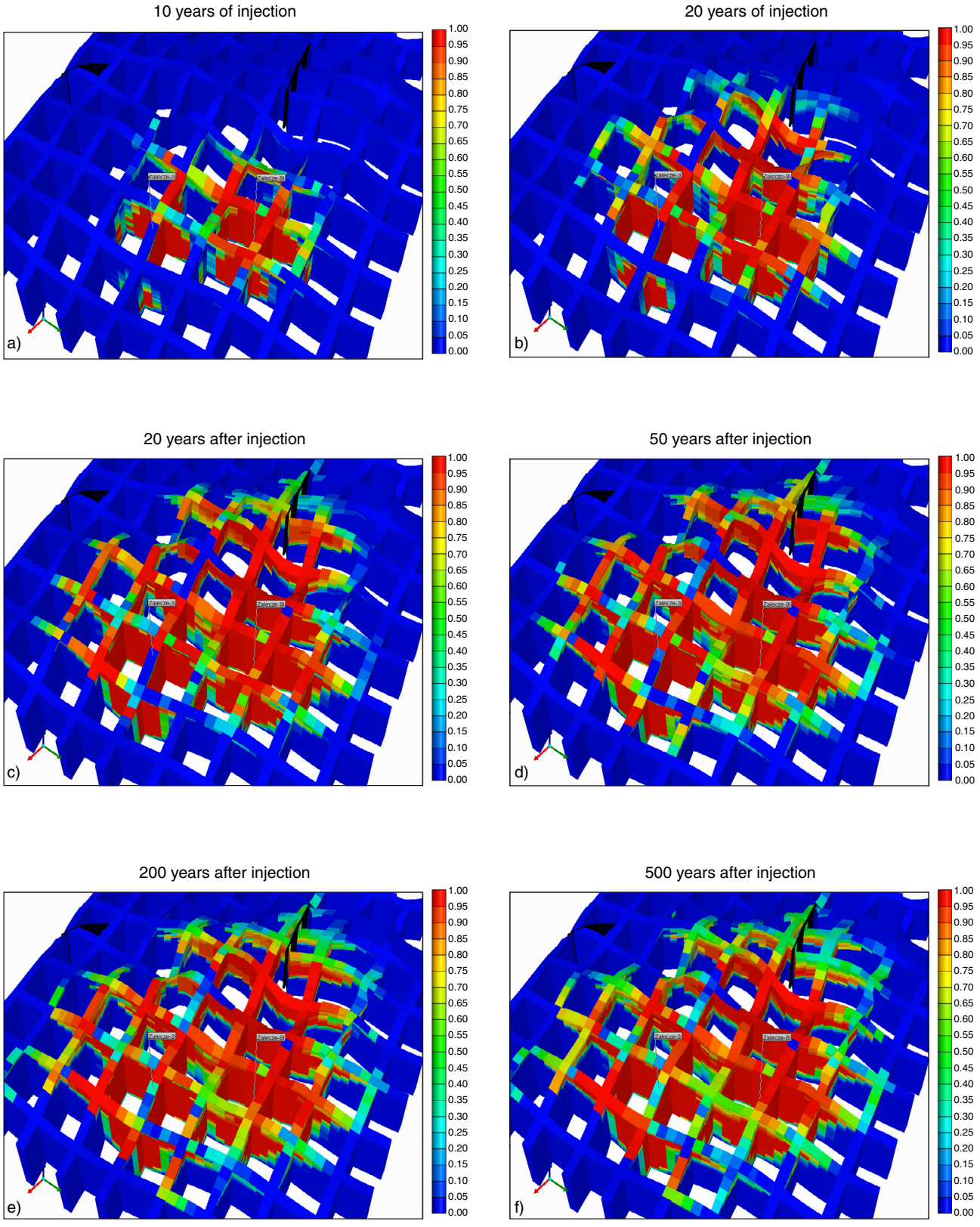

Figure 7

CO_2 mole fraction in the Załęcze reservoir after a) 10 years and b) 20 years of injection, and c) 20 years, d) 50 years, e) 200 years and f) 500 years after the end of the CO_2 injection period.

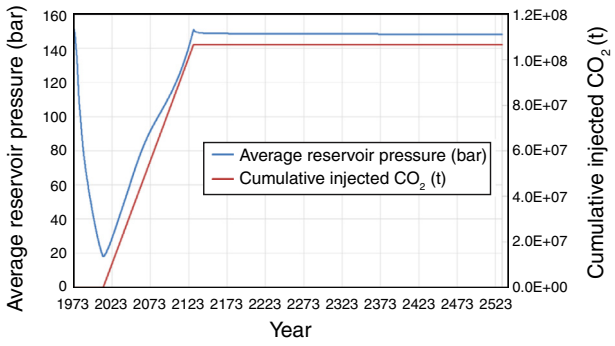

Figure 8

Reservoir pressure development and amount of injected CO_2 in the second simulation scenario.

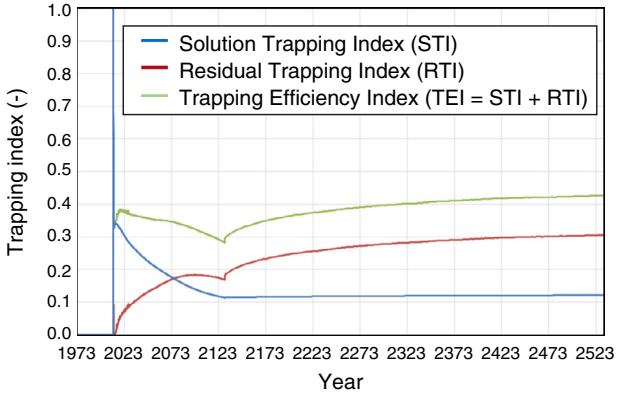

Figure 9

Trapping dynamics during the long-term injection and post-injection periods in the second simulation scenario.

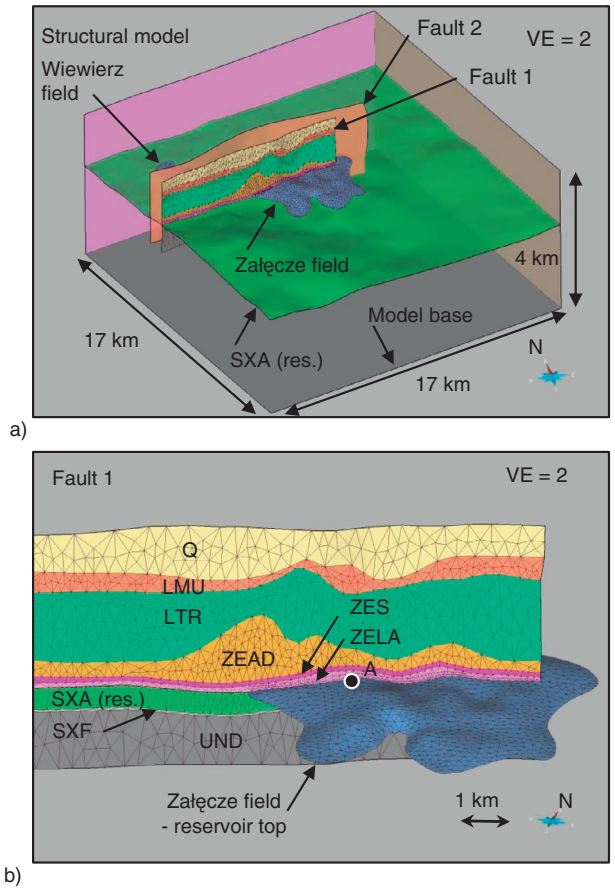

Figure 10

a) Structural framework model of the Załęcze gas field used to build a finite element mesh for the geomechanical model. b) Enlarged view of the regional Fault 1 intersecting the Załęcze gas reservoir. Legend: Q, Quaternary; LMU, Lower Muschelkalk; LTR, Lower Triassic; ZEAD, Zechstein anhydrites and dolomites; ZES, Zechstein salt; ZELA, Zechstein Lower anhydrite; SXA, Saxonian aeolian reservoir; SXF, Saxonian fluvial Sandstone; UND, Underburden; VE, vertical exaggeration.

3.1.1 Methodology

A field-scale hydro-mechanical numerical model of the Załęcze reservoir was built from the regional structural geological model of the study area developed by Papiernik *et al.* (2012). The regional model (50 km × 20 km) incorporates the two major gas reservoirs in the area, the Załęcze and Żuchlów gas fields, while the field-scale hydro-mechanical model incorporates only the Załęcze field, and therefore has a smaller spatial extent (17 km × 17 km × 4 km). The hydro-mechanical model comprises the lithological units with assigned material properties and constitutive laws, the initial stress state and the pore pressure of the reservoir based on gas extraction and subsequent CO_2 injection. A one-way hydro-mechanical coupling was used, assuming that pore pressure changes induce stress changes, while the induced stress changes and associated deformation do not influence the dynamic flow. The calculations were performed with the finite element package DIANA (TNO Diana, 2012).

3.1.2 Model Implementation

A field-scale geomechanical model of the Załęcze gas field was implemented from the structural framework of horizons and faults interpreted within the model domain (Fig. 10a). The 130-m-thick main gas reservoir, composed of the Zechstein carbonates (Ca1) and the Saxonian aeolian and Fluvial sandstones, is located approximately in the centre of the modeled domain to minimise the effects of model boundaries on induced stresses associated with gas production and subsequent CO_2 injection in the main reservoir.

TABLE 4
Parameterisation of geomechanical units implemented in the field-scale hydro-mechanical model

Geological unit	Geomechanical unit	Density (kg/m^3)	Elastic modulus (GPa)	Poisson's coefficient (-)	Newtonian viscosity (Pa.s)
Quaternary	Overburden 1	2 000	5	0.3	–
Muschelkalk	Overburden 2	2 300	10	0.3	–
Buntsandstein	Overburden 3	2 300	15	0.3	–
Upper Zechstein anhydrite	Caprock secondary	2 500	22	0.25	–
Zechstein Salt	Caprock primary	2 170	30	0.26	–/6.4E+16
Lower Zechstein anhydrite*	Caprock primary	2 950/2 170	28/30	0.31/0.26	–/6.4E+16
Carbonate Ca1	Reservoir	2 760	39	0.18	–
Saxonian aeolian sandstone	Reservoir	2 410	13	0.23	–
Saxonian fluvial sandstone	Reservoir	2 670	21	0.23	–
Carboniferous	Underburden	2 650	30	0.25	–
Faults	Normal stiffness (GPa/m)	Shear stiffness (GPa/m)	Friction coefficient (-)	Dilation coefficient (-)	Cohesion (MPa)
	20	20	0.6	0.087	0

* In the scenario assuming a viscoelastic caprock, the Lower Zechstein anhydrite has the same properties as the Zechstein salt.

The model was rotated in the horizontal plane 20° counterclockwise from the North to align the model boundaries with the regional directions of the principal horizontal stresses in the area (Heidbach *et al*., 2008).

The hydro-mechanical model consists of ten layers: three overburden layers, three layers comprising the top seal, three reservoir layers and one underburden layer (Tab. 4). 295 000 quadratic second-order ten-node solid pyramid elements were used to represent the geological layers. Two regional subvertical faults, east-northeast-striking, were implemented in the hydro-mechanical model (Fig. 10b). The faults at the reservoir level have small vertical offsets and do not affect cross-fault gas flow in the reservoir. The fault surfaces were modeled by 6 000 triangular second-order 6 + 6 noded planar interface elements of zero thickness.

The lithological units were assumed to be purely elastic except for the Zechstein salt layer, which was modeled as a viscoelastic material (Tab. 4). The values of the elastic properties for the reservoir rock were derived from uniaxial compressive strength tests executed in the rock mechanics laboratory of the AGH University of Science and Technology in Cracow; the values for the other layers were derived by interpretation of well logs from the Załęcze-6 well.

The Zechstein salt layer was modeled as a solid viscoelastic material with an effective Newtonian viscosity of 6×10^{16} Pa.s. The value for the Newtonian viscosity was derived from available literature on deep solution salt mining (van Heekeren *et al*., 2009). The chosen Newtonian viscosity used in the simulations agrees, within one order of magnitude, with the experimental data obtained during very slow creep tests under low differential stresses (< 1 MPa) reported by Bérest *et al*. (2005, 2014). We adopted the same value for simulations of the steady-state creep in salt as low differential stresses are also expected to develop in the Zechstein salt caprocks as a consequence of pore pressure changes in the main gas reservoir. The frictional behaviour of the faults is modeled using the Coulomb failure criterion with a friction coefficient of $\mu = 0.6$ and zero cohesion.

The initial stress state was introduced assuming a normal-faulting stress regime. In the absence of field data, the magnitude of the minimum horizontal stress was determined from the assumption that faults, which are optimally oriented for slip, are critically stressed.

In this case, the effective stress ratio (*i.e*. the ratio of horizontal-to-vertical effective stress) amounts to $K_0' = \sigma_h'/\sigma_v' = 0.32$ for a friction coefficient value of $\mu = 0.6$ (Jaeger *et al*., 2007). We used a slightly lower value

of $K_0' = 0.3$ as the faults implemented in the hydro-mechanical model are subvertical, and therefore not critically oriented for slip. The geomechanical model was initialised by applying a gravitational load and an initial pore pressure of 15 MPa in the Załęcze reservoir, using a nonlinear iterative procedure. Transient loading of the Ca1 Carbonate reservoir and the Saxonian reservoirs was achieved by applying uniform pressure changes throughout the entire gas cap. During the past 30 years of gas production the reservoir pressure was decreased by 95% from 15 MPa to 0.75 MPa. The pressure remained constant over the next two years of no activity. A CO_2 injection phase of 10 years' duration followed, during which the reservoir was repressurised up to 13.5 MPa, *i.e.* 90% of the initial reservoir pressure.

3.1.3 Simulation Results and Discussion

The stress initialisation procedure described in the previous section was suitable for the case of a purely elastic response of all lithological model units (*i.e.* the elastic case). Such a standard procedure, which is, for example, commonly used in geotechnical engineering, is often not satisfactory for the initialisation of stresses in viscous salt layers. The intrinsic characteristic of a viscoelastic material is that it cannot sustain differential stresses in the long term, while the standard initialization procedure cannot remove the differential stresses from the salt layers to a negligible level, *i.e.* below a few tenths of one MPa (Fig. 11a). In order to achieve the required level of stress relaxation, we carried out transient computations with the active gravitational load and creep behaviour of salt. The stresses in the sediments were allowed to equilibrate over 30 years of simulation time, while the prescribed stress ratios in the salt layer ($K_0' = K_0 = 1$) and the other layers ($K_0' = 0.3$) were matched. This was sufficient to reach the initial model equilibrium and remove the initially large differential stresses from the salt layer. The remaining differential stresses in the Zechstein salt layer after 30 years of simulation time were close to zero (Fig. 11b).

The simulation scenarios considered different constitutive behaviour of the caprock salt layer and different sealing behaviour of the faults. Four simulations were performed under the following assumptions:

- an elastic caprock and repressurisation of the whole reservoir;
- an elastic caprock and partial repressurisation of the reservoir caused by the sealing behaviour of the reservoir faults;
- a viscoelastic salt caprock and repressurisation of the whole reservoir;
- a viscoelastic salt caprock and partial repressurisation of the reservoir.

The simulation results were analysed by comparing the induced deformation and the effects on fault integrity

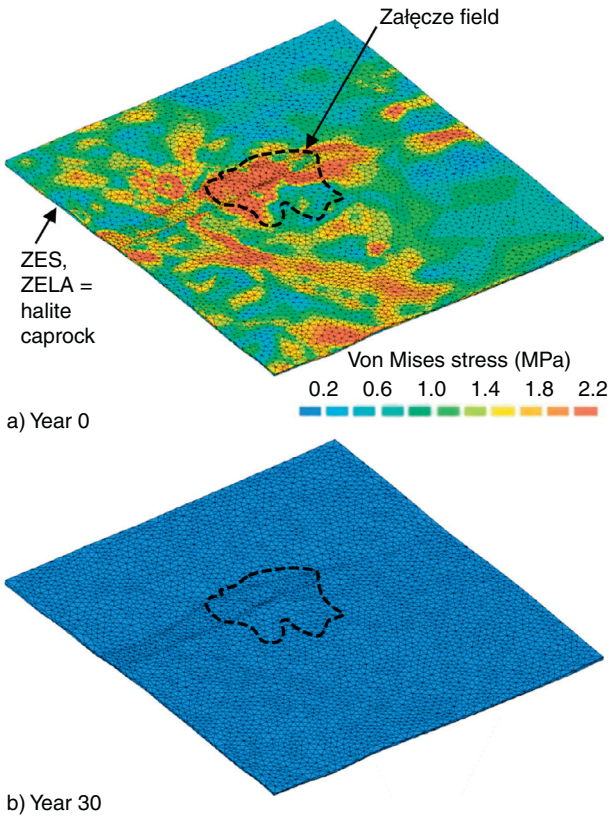

Figure 11

Field-scale simulation results showing Von Mises stresses in the halite caprock a) after model initialisation; and b) after 30 years of stress equilibration. Salt-sediment interaction leads to a full relaxation of differential stresses in the halite caprock.

influenced by gas production and subsequent CO_2 injection. Due to the lack of subsidence monitoring data from the production period, it was not possible to calibrate the hydro-mechanical model to the measured subsidence.

The induced deformation is the largest at the end of the gas production period. The maximum amount of surface subsidence obtained using the elastic caprock model is relatively small with 4.5 cm. This is due to the small thickness of the gas-bearing, compacting reservoir layers (average thickness 40 m; range 20 m to 110 m) applied in the field-scale hydro-mechanical simulation model as well as the presence of a stiff carbonate layer in the upper part of the reservoir and a stiff anhydrite layer in the primary caprock. Furthermore, the absence of depletion in the supporting aquifers additionally limits the maximum subsidence. Surface subsidence is lower than reservoir compaction (4.5 cm *versus* 7.2 cm; Fig. 12). This can be attributed to the stress transfer (*i.e.* the stress arching), which occurs above a compacting reservoir of a finite size. Reservoir compaction causes unloading

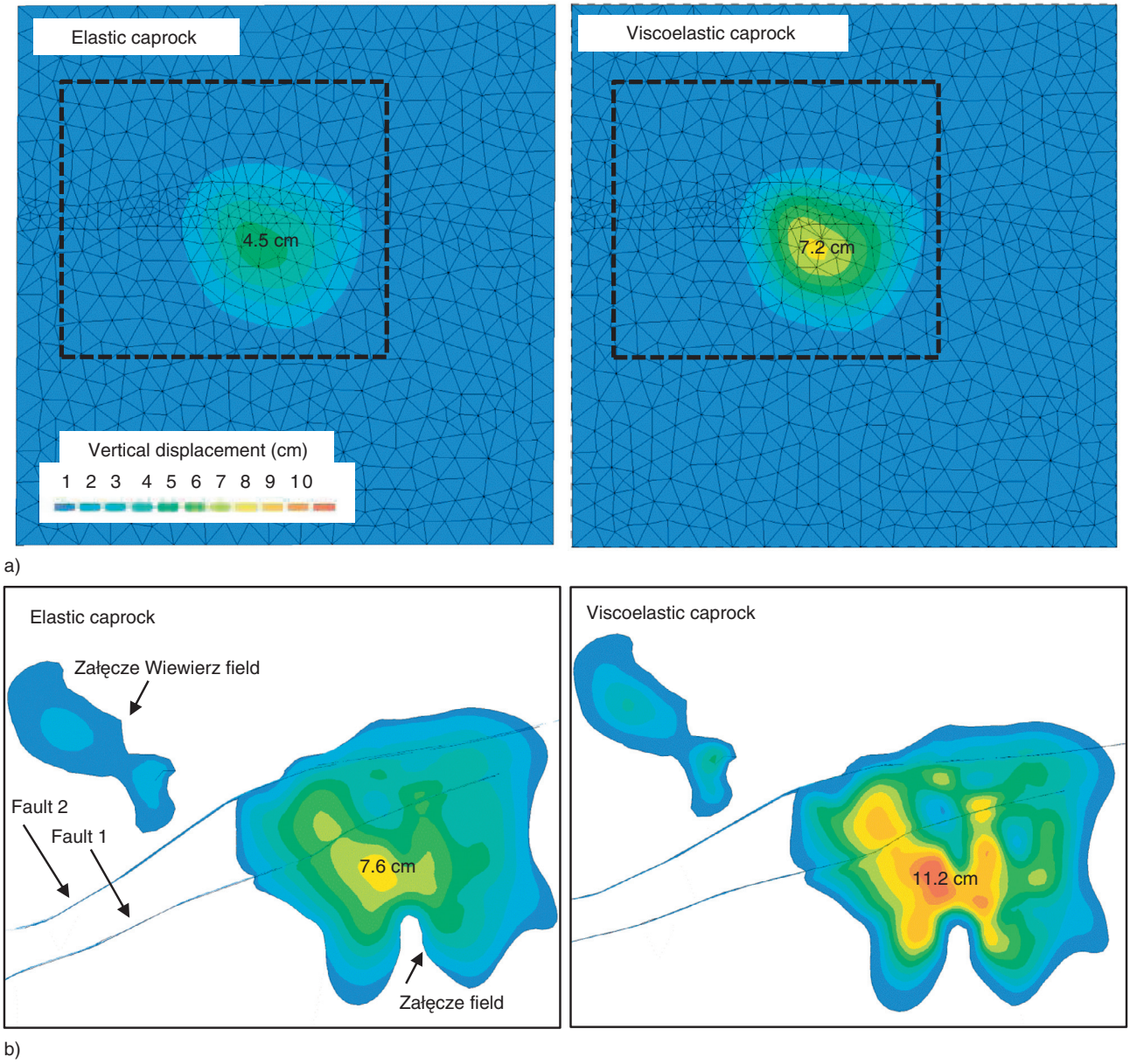

Figure 12

a) Contour plots comparing depletion-induced vertical displacements predicted by the model with an elastic caprock and the model with a viscoelastic caprock. a) Surface subsidence and b) reservoir compaction at the end of the depletion period. The model with a viscoelastic caprock predicts larger deformations.

(*i.e.* a decrease in compressive stresses and decompaction) of the layers above the reservoir and loading of the sediments near the reservoir edges. Due to the finite extent of the reservoir, the loaded part of the side-seal near the reservoir edges takes over a part of the overburden load previously borne by the undepleted reservoir, resulting in a surface subsidence below reservoir compaction.

Remarkably, the maximum amount of surface subsidence is 60% larger for the case of a viscoelastic caprock (7.2 cm) compared with the case of an elastic caprock (4.5 cm; Fig. 12). The presence of a viscoelastic layer above a compacting reservoir results in a subsidence bowl (*i.e.* depression), which is commonly narrower and deeper than the subsidence bowl obtained for the case of an elastic

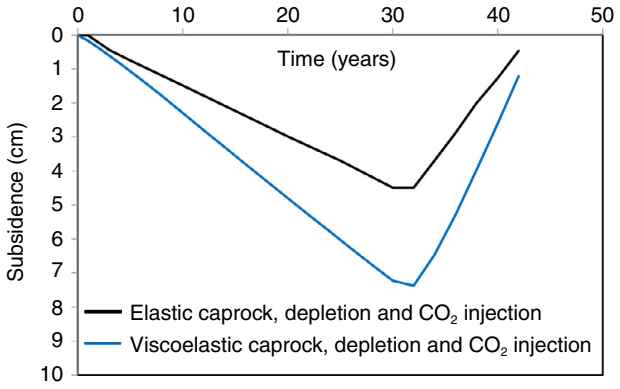

Figure 13

Maximum surface subsidence over time in the field-scale hydro-mechanical models with elastic and a viscoelastic caprocks.

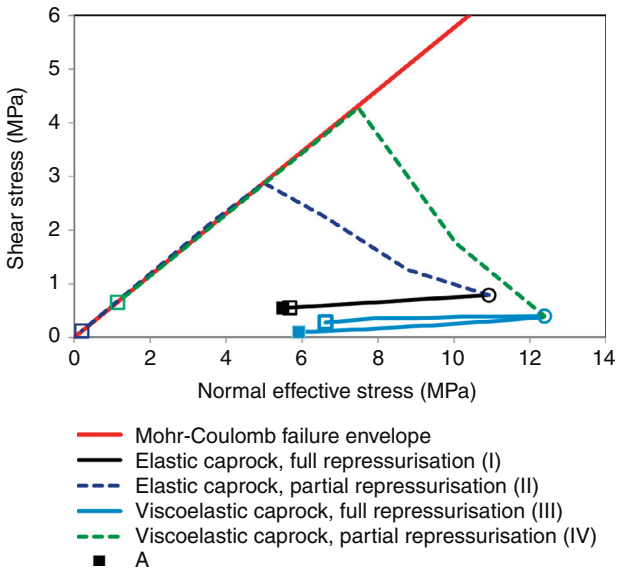

Figure 14

Stress paths for Point A located on the reservoir section of Fault 1 (shown in Fig. 10). The stress paths are shown for the model with an elastic caprock assuming repressurisation of the whole reservoir (I) and partial reservoir repressurisation (II); and for the model with a viscoelastic caprock assuming repressurisation of the whole reservoir (III) and partial reservoir repressurisation (IV). Solid arrows show the stress development during depletion, dashed arrows during injection. The initial stress state is shown by filled squares, the state of stress after depletion by open circles and that after CO_2 injection by open squares. Hydro-mechanical analyses demonstrate that the sealing Fault 1 can be destabilised at the level of the reservoir in the highly unlikely case of a partial reservoir repressurisation (II and IV).

subsurface (Orlic and Wassing, 2013). Another important difference is that the salt continues to deform after the cessation of production or injection activities until a full dissipation of differential stresses from the salt is reached. As a consequence, the shape of the subsidence bowl even changes after the end of injection or production operation. Such residual subsidence can be observed during the two-year shutdown period after the cessation of gas production (Fig. 13). Repressurisation of the depleted Załęcze reservoir to 90% of the initial pore pressure largely reduces and reverses the stress changes and associated deformation induced by depletion. The maximum subsidence remaining after the CO_2 injection is small: 0.5 cm for the case of an elastic caprock and 1.2 cm for the case of a viscoelastic caprock (Fig. 13).

A stress-path plot is used to demonstrate the evolution of stresses on the faults during the simulations of different scenarios (Fig. 14). The stress path is plotted for Point A, which is located at the reservoir intersection with Fault 1 (Fig. 10b). Because the faults implemented in the hydro-mechanical field-scale model are subvertical, the shear stresses on the faults are initially low (shown by solid squares in Fig. 14) and far away from the assumed Coulomb failure envelope. The paths for depletion (shown by solid lines starting from the solid squares and ending on the open circles) show an increase in normal effective stress by several MPa, but hardly any increase in shear stress. The stress path for the case of a viscoelastic caprock (III) is slightly shifted compared with the case of an elastic caprock (I), but still very similar. In all cases, the stress paths for depletion remained far from the failure envelope, which suggests that the faults did not slip at the observation point during the gas production phase.

CO_2 injection largely reverses the stress changes induced by gas production. This is demonstrated by the stress paths for injection, which are shown by dashed lines starting from the open circles and ending on the open squares in Figure 14. In the cases of a uniform repressurisation of the whole reservoir, the stress paths for injection fully overlap (elastic case, I), or are very close (viscoelastic case, IV) to the corresponding stress paths for depletion. The final stress state on the faults is very similar to the pre-depletion stress state. Apparently, the fault integrity is not affected by repressurisation of the whole reservoir.

The additional two simulations (II, IV) considered a hypothetical case of partial reservoir repressurisation. Such a scenario is highly unlikely for the Załęcze reservoir as there was no evidence of reservoir compartmentalisation during gas production. However, here we use this scenario to demonstrate the hydro-mechanical effects resulting from repressurisation of a single reservoir compartment.

In scenarios II and IV, the CO_2 injection in the depleted reservoir causes repressurisation of a single reservoir block, while the neighbouring reservoir block remains depleted. Differential deformation of the reservoir blocks on either side of the fault leads to fault slip, which is shown by the stress path evolution towards and along the failure envelope (the paths II and IV in Fig. 14, shown by the dashed lines starting from the open circles and ending on the open squares).

3.2 Regional-Scale Hydro-Mechanical Simulation Strategy

Using spatial pore pressure distribution from the history-matched dynamic flow simulations discussed in Section 2, we carried out one-way coupled hydro-mechanical simulations using a regional-scale numerical model to account for the second dynamic flow simulation scenario considering CO_2 injection starting about 39 years (2012) after initial natural gas production (1973) and continuing for about 118 years (2130) together with gas production until the initial reservoir pressure of 15.1 MPa is achieved again. The main aim of the present hydro-mechanical regional-scale simulation study was to investigate the reservoir, caprock and fault integrity on a regional scale, taking into account 31 faults mapped by Papiernik *et al.* (2012) located in the model domain.

3.2.1 Methodology

We implemented a regional-scale hydro-mechanical numerical model based on the regional structural geological model discussed by Papiernik *et al.* (2012) with a spatial extent of about 29 km × 28 km × 5 km. A one-way hydro-mechanical model coupling was applied using the upscaled pore pressure distribution derived from the history-matched dynamic flow simulation model (8.1 km × 8.6 km × 220 m) for 15 coupled simulation time steps. The finite-difference software package FLAC3D (Itasca, 2013) was applied for the simulations.

3.2.2 Model Implementation

The regional-scale hydro-mechanical model is discretised by 108 × 118 × 136 hexahedral elements summing up to a total of 1 733 184 elements and 1 777 027 nodes (Fig. 15). The vertical discretisation is determined by four zones with the overburden consisting of 26 elements of 32 m thickness, the Ca1 Carbonate reservoir, Saxonian aeolian and Saxonian fluvial sandstones of 50 elements of 16 m thickness, as well as two different underburden zones with 21 and 39 elements of 32 m and 64 m thickness, respectively (Fig. 15).

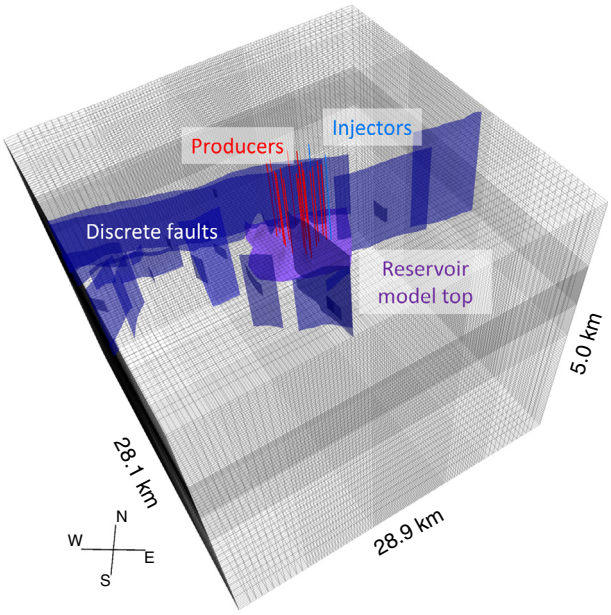

Figure 15

Discretisation of the regional-scale hydro-mechanical model including 31 discrete faults (blue), the dynamic flow reservoir model (magenta), 19 natural gas production wells (red) and two CO_2 injection wells (light blue). Vertical exaggeration by a factor of 5.

All 31 regional faults mapped by Papiernik *et al.* (2012) and located within the boundaries of the regional-scale hydro-mechanical model were integrated to carry out a comprehensive fault slip and dilation tendency analysis (Fig. 16). Furthermore, twelve geological units were implemented into the hydro-mechanical model. The entire model grid was rotated by 35° (counter-clockwise) to apply the regional stress field reported by Jarosinski (2005a,b) as the initial stress state, as discussed in the following paragraphs.

The FLAC3D Mohr-Coulomb model allowing for elasto-plastic material behaviour was applied to all lithological units using the data listed in Table 5. Hereby, different elastic moduli, Poisson's coefficients and friction angles determined in sensitivity analyses were used for the Zechstein halite and Zechstein salt to establish an isotropic stress state in these salt rock units representative of the absence of shear stresses (low differential stresses). The discrete faults were implemented as ubiquitous joint elements as discussed by Kempka *et al.* (2015); the exact fault dip direction and dip angle are considered for the associated weak planes. Fault properties are determined by a cohesion of 0 MPa, a friction angle of 31° (equals a friction coefficient of 0.6) according to Jaeger *et al.* (2007) and dilation angle of 10° (equals a dilation coefficient of 0.176). The parameters for

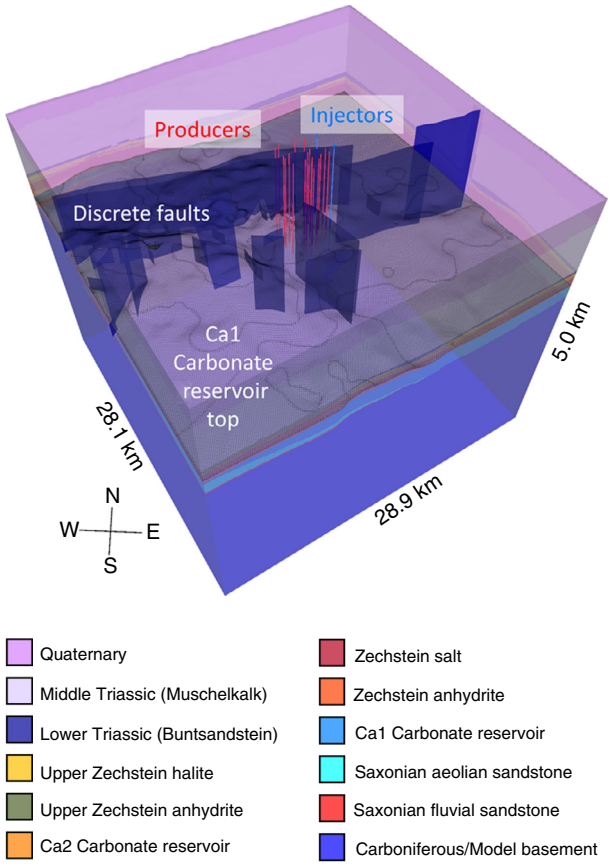

Figure 16

Lithological units integrated into the regional-scale hydro-mechanical model including the 31 discrete faults (blue), the Ca1 Carbonate reservoir top (internal gridded surface), 19 natural gas production wells (red) and two CO_2 injection wells (light blue). Vertical exaggeration by a factor of 5.

the reservoir units were provided by AGH University of Science and Technology as discussed before. All other mechanical parameters were derived from Kempka *et al.* (2014), Ouellet *et al.* (2010), Nagelhout and Roest (1997) and internal discussions.

A normal faulting stress regime with a maximum horizontal stress $S_{H\max} = 0.89\ S_V$ (vertical stress) and $S_{H\max} = 1.25\ S_{h\min}$ (minimum horizontal stress) was identified by Jarosinski (2005b) in the Grochowice-3 well at a depth between 1 634 m and 1 639 m located about 87 km west of the Załęcze gas field. Using the pore pressure data determined at that depth to 1.7 MPa, the effective horizontal to vertical stress ratio can be calculated as $K_0' = \sigma_h'/\sigma_v' = 0.50$.

Jarosinski (2005a) investigated the regional stress field by a well breakout analysis summarising $S_{H\max}$ orientations for different well locations in the Fore-Sudetic Monocline. The Paproc-29 (150° ± 13° at 1 388 m to 1 425 m depth, quality D) and the Wierzchowice-1 wells (112° ± 10°, 660 m to 1 260 m depth, quality E) located about 150 km northwest and 65 km east of the Załęcze gas reservoir, respectively, were considered in the determination of the $S_{H\max}$ azimuth. However, the low quality of the well breakout measurements documented by Jarosinski (2005a) leads us to prefer the regional stress field as a more reliable indicator for the $S_{H\max}$ azimuth given with 145° ± 17°. This value is in good agreement with the data determined for the Paproc-29 well at the Ca1 reservoir depth range. Consequently, a $S_{H\max}$ azimuth of 145° was assumed for the hydro-mechanical simulations discussed in the following, so that the numerical model grid had to be rotated by 35° (clockwise) in advance of the initial stress application in order to allow for a normal stress assignment at the model boundaries. Normal displacements at the lateral and bottom model boundaries were fixed, while the model top was allowed to displace in any direction. The regional-scale hydro-mechanical model was then calibrated under consideration of a gravitational load to the aforementioned stress state at the Ca1 reservoir top using the initial spatial pore pressure distribution derived from the dynamic flow simulations, and then fully equilibrated in an iterative approach involving multiple simulation runs.

3.2.3 Simulation Results and Discussion

Resulting from equilibration with different material properties for the halite and salt rock units, a sufficiently low differential stress was achieved in the respective lithological units (0.22 MPa to 0.37 MPa). Since monitoring of ground surface displacements was not carried out throughout the entire production time, a model calibration based on these data was not possible. Figure 17 plots the simulated maximum vertical displacements at the Ca1 reservoir top and the ground surface. Until the start of CO_2 injection *via* two wells in 2012, maximum vertical displacements of about −14.4 cm at the Ca1 reservoir top and of about −11.6 cm at the ground surface are achieved. Absolute maximum vertical displacements are encountered in 2022 (10 years after the start of CO_2 injection) with −14.7 cm (Ca1 reservoir top) and −11.8 cm (ground surface). Thereafter, the effect of pore pressure increase by CO_2 injection overcomes the pore pressure decrease induced by natural gas production from 19 wells, and thus the induced subsidence is decreased by the competing ground uplift. At the end of operation (2130), the remaining maximum vertical displacements were calculated to be −4.8 cm (Ca1 reservoir top) and −2.8 cm (ground surface). Since the two CO_2 injection wells are perforated below the gas-water contact, CO_2 is still migrating and increasing the pore pressure in the gas cap after the end of CO_2 injection and natural gas production. As a consequence, ground uplift continues, resulting in a maximum

TABLE 5
Applied material properties in the regional-scale hydro-mechanical simulation model

Lithological unit	Elastic modulus (GPa)	Poisson's coefficient (-)	Friction angle (°)	Cohesion (MPa)	Tensile limit (MPa)	Density (kg/m^3)
Quaternary	5.0	0.4	35	0	0	2 100
Middle Triassic (Muschelkalk)	26.0	0.18	25	5	5	2 650
Lower Triassic (Buntsandstein)	27.0	0.26	25	5	5	2 450
Upper Zechstein halite	1*/22	0.40*/0.25	1*/25	0	0	2 060
Upper Zechstein anhydrite	27.0	0.26	30	5	5	2 600
Ca2 Carbonate reservoir	27.0	0.26	30	5	5	2 450
Zechstein salt	1*/28	0.40*/0.26	1*/0.26	0	0	2 170
Zechstein anhydrite	28.0	0.31	30	5	5	2 950
Ca1 Carbonate reservoir	39.0	0.18	30	5	5	2 760
Saxonian aeolian sandstone	13.0	0.23	30	5	5	2 410
Saxonian fluvial sandstone	21.0	0.23	30	5	5	2 670
Carboniferous/ model basement	30.0	0.19	30	5	5	2 700

* Values applied for equilibrium run.

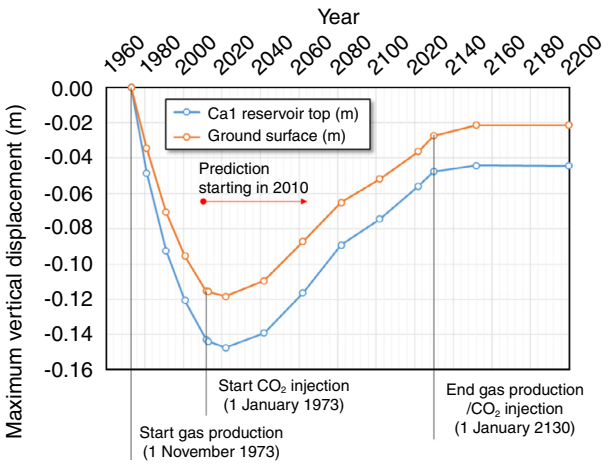

Figure 17

Calculated maximum vertical displacements (m) at the Ca1 reservoir top and ground surface during natural gas production (1973-2130) and CO_2 injection (2012-2130).

vertical displacement of −4.45 cm (Ca1 reservoir top) and −2.13 cm (ground surface) after 2152. This equals a reduction in absolute maximum subsidence by about 69% (Ca1 reservoir top) to 82% (ground surface) as a result of EGR by simultaneous CO_2 injection.

Figure 18 shows a plane view of vertical displacements at the Ca1 reservoir top and ground surface for selected time steps. One year after the start of CO_2 injection (2013), a trend of positive (upward) vertical displacements can be identified in the vicinity of the two CO_2 injection wells. This uplift footprint becomes more evident in 2042 and thereafter (2042 and 2062). As a result of ongoing CO_2 migration after the CO_2 injection shutdown in 2130, spatial vertical displacements are further reduced at the Ca1 reservoir top.

The spatial effect of CO_2 injection on subsidence mitigation is also observed at the ground surface: while an almost radial subsidence bowl with a slight deviation in the northeast (resulting from reservoir topography and the two major faults at this location) is observed in 2012, a ground uplift

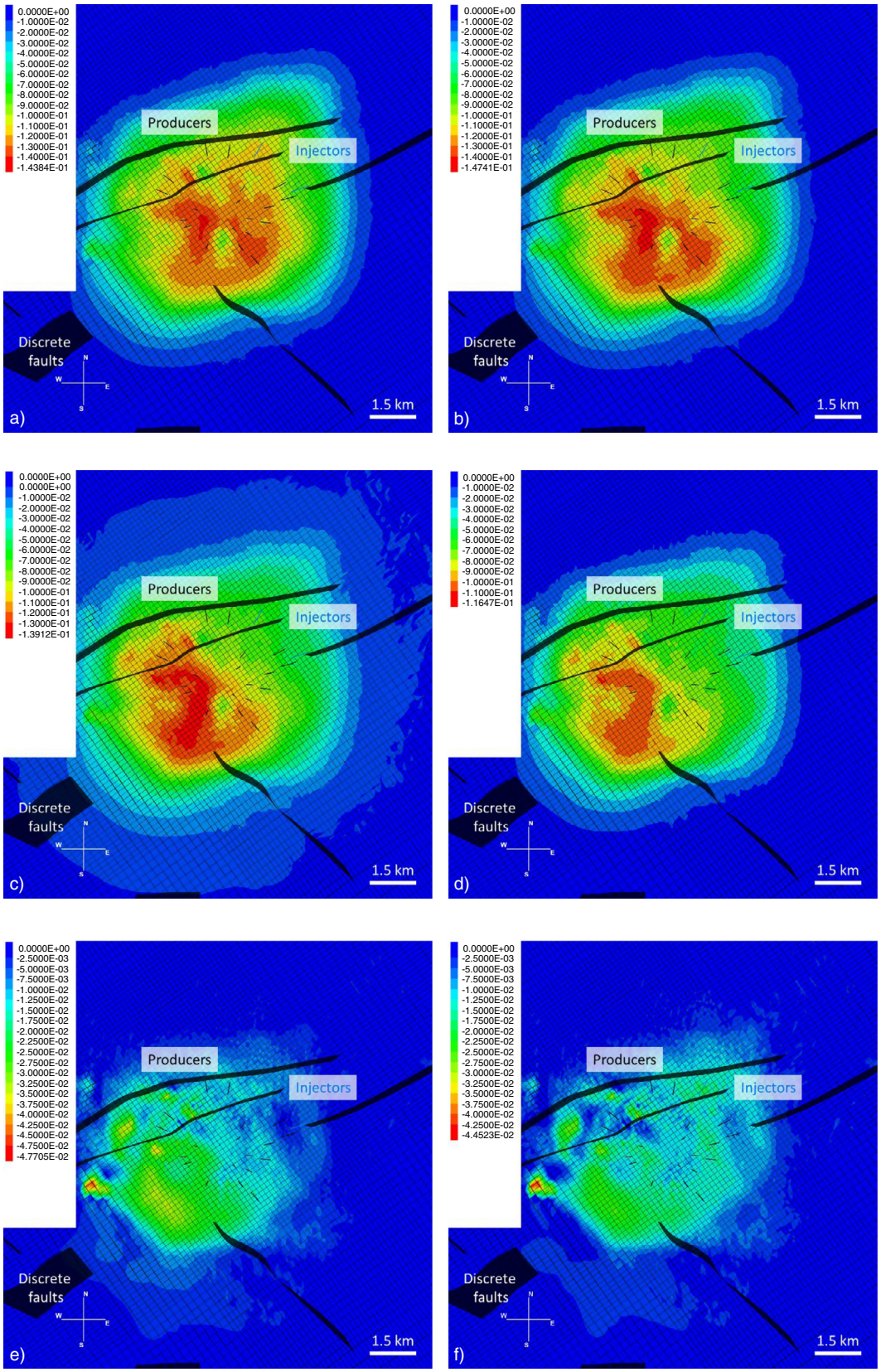

Figure 18

Plane view of vertical displacements (m) at the Ca1 reservoir top in a) 2012, b) 2022, c) 2042, d) 2062, e) 2130 (end of operation) and f) 2200.

can be observed in the vicinity of the two CO_2 injection wells in 2022. This trend continues until the end of operation in 2130. As discussed before, the CO_2 is still migrating in the reservoir, resulting in a final hydro-mechanical equilibrium until 2152 (Fig. 19).

Comparing the simulation results on vertical displacements between the field-scale (Sect. 3.1) and regional-scale (this section) hydro-mechanical models, notable deviations can be pointed out: *e.g.* the vertical displacements at the reservoir top calculated by the field-scale simulation model are about 31% (viscoelastic model) to 93% (purely elastic model) lower compared with the regional-scale model simulation results. These apparently high deviations are mainly a product of the chosen constitutive laws: the FLAC3D Mohr-Coulomb model allows for irreversible deformation (plastification) in all lithological units implemented in the hydro-mechanical model. As discussed in the following, the reservoir section is subject to significant spatial plastification in the reservoir area according to the regional-scale simulations resulting from the relatively high changes in effective stresses as a consequence of reservoir depletion (pore pressure decrease from 151 bar to below 20 bar). The influence of the chosen constitutive laws is already obvious when comparing the simulation results produced with the field-scale hydro-mechanical model (Sect. 3.1), in which purely elastic and viscoelastic constitutive laws were applied. Here, allowing plastic deformation (more precisely creep) in the Zechstein salt seal only (not as in the regional-scale model in all units) already increases the vertical displacements by 60% compared with the purely elastic case.

Another relevant reason for the deviations in calculated vertical displacements is that, in the field-scale model, pore pressure changes were only considered in the gas cap (Fig. 10b) while constant pore pressure was maintained in all other lithological units. However, the regional-scale model considers the entire spatial pore pressure distribution calculated by the dynamic flow simulations (Sect. 2) for different time steps and the entire Ca1 Carbonate reservoir as well as both Saxonian sandstone units. Consequently, the impact of pore pressure changes is significantly higher in the regional-scale simulation case. We do not expect the differences in the parameterisation of the Triassic units between the two simulation strategies to be responsible for the deviations in vertical displacements discussed above.

Shear failure experienced at the faults as well as plastification (irreversible deformation) in the lithological units located in the natural gas reservoir (Ca1 Carbonate reservoir and Saxonian aeolian sandstones) are plotted in Figure 20. Due to the significant pore pressure decrease resulting from natural gas production from 19 production wells (from about 151 bar to below 20 bar, Fig. 8) all fault shear failure and almost all reservoir plastification are encountered before CO_2 injection starts in 2012. No additional fault slip and only minor additional reservoir rock plastification is observed thereafter until the end of operation in 2130. Fault shear failure is observed at the depth of the Middle Triassic (Muschelkalk) unit at the two faults cutting the Załęcze gas field and at reservoir depth for the northwest-striking fault in the South of the Załęcze gas field. Plastification is not encountered at any location above or below the natural gas reservoir, indicating that caprock integrity is not compromised, while the significant plastification of the reservoir rock is mainly responsible for the higher vertical displacements at the reservoir top during the natural gas production period compared with the field-scale model, as discussed before (Fig. 18). Since fault reactivation is limited to the reservoir units (Ca1 Carbonate reservoir as well as Saxonian aeolian and fluvial sandstones) and the Middle Triassic only, potential leakage pathways for formation fluids, natural gas or injected CO_2 cannot be identified based on the simulation results. Co-injection of CO_2 during natural gas production supports the reservoir integrity by increasing pore pressure, and hence effective normal stresses on the faults, decreasing fault slip tendency.

Fault slip and dilation tendencies are plotted for two different views in Figures 21 and 22. The maximum initial fault slip tendency is about 0.52 and not exceeding 0.6 at any of the faults during the entire simulation time. At the depth of the first (Zechstein) and second caprocks (Upper Zechstein), the fault slip tendency is close to zero during the entire simulation time as a result of the low initial differential stresses. This strongly supports the present theory that the supra- and subsaliniferous fault systems are independent and not connected to each other, as discussed by Papiernik *et al.* (2012). Furthermore, these results are in good agreement with the field-scale simulation strategy results, with the slip tendency decreasing at the interface of the Ca1 Carbonate reservoir to the Zechstein anhydrite (Point A in Fig. 10b), with maximum slip tendencies being below 0.2 for the initial and full repressurisation cases (Fig. 14).

Fault areas experiencing failure (Fig. 20) exhibit an increased slip tendency with maximum values up to 0.6. The dilation tendency is close to one in the Zechstein caprocks at the initial stress and pore pressure states, but decreases to about 0.5 to 0.6 when the minimum reservoir pressure is almost reached after 2013. The northwest-striking fault in the South of the Załęcze gas field exposes a notably high dilation tendency over its entire area as a result of its parallel orientation to the $S_{H\max}$ azimuth. However, the dilation tendency at the depth level of the Zechstein caprocks is also decreased for this fault due to the reduction in reservoir pore pressure. In summary, the fault slip and dilation tendency as well as the fault shear failure analysis demonstrate that continuous vertical leakage pathways along the fault systems connecting the reservoir units (Ca1 Carbonate reservoir and Saxonian Rotliegend reservoirs) to shallower units or freshwater aquifers are unlikely

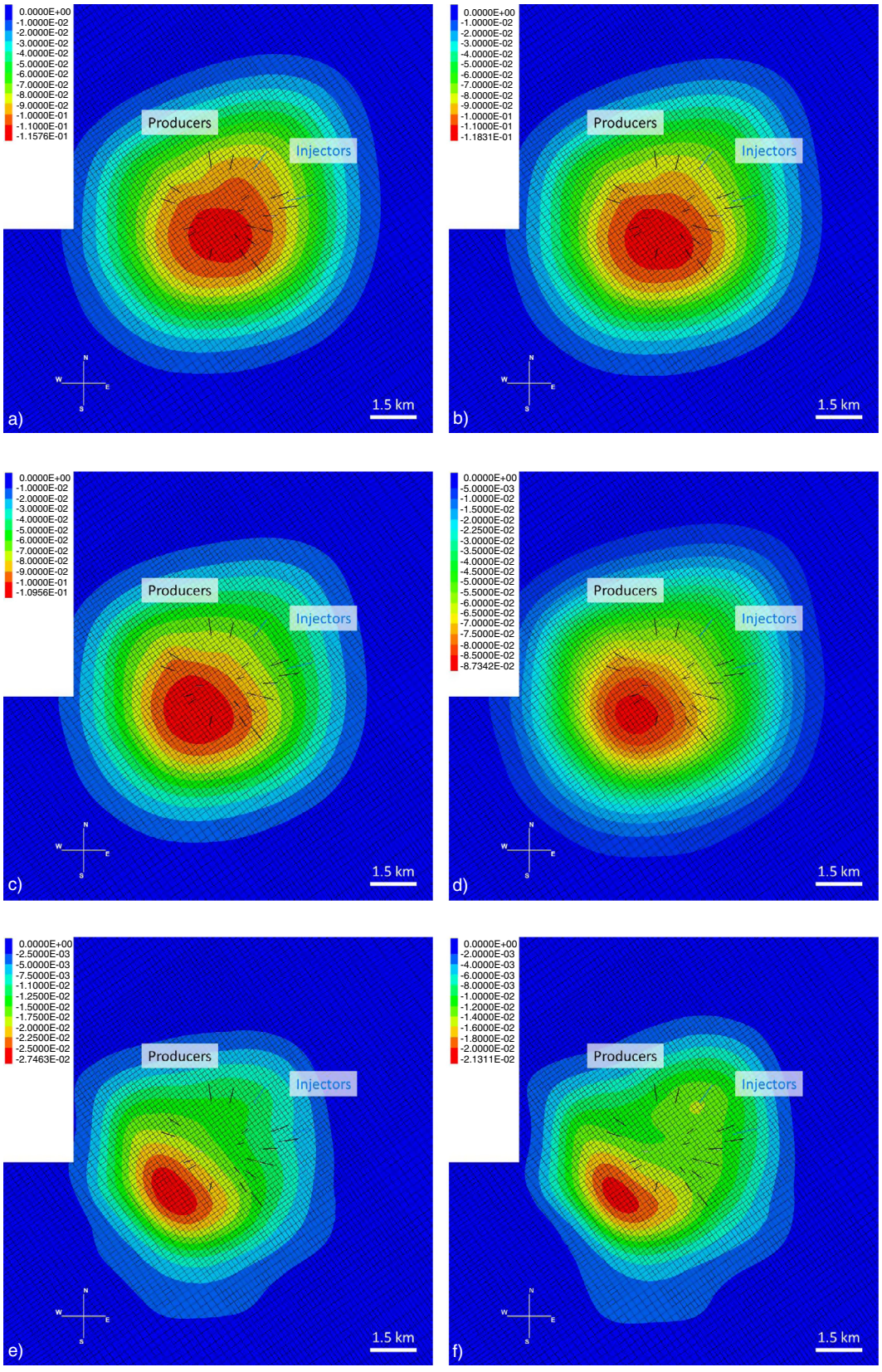

Figure 19

Plane view of vertical displacements (m) at the ground surface in a) 2012, b) 2022, c) 2042, d) 2062, e) 2130 (end of operation) and f) 2200.

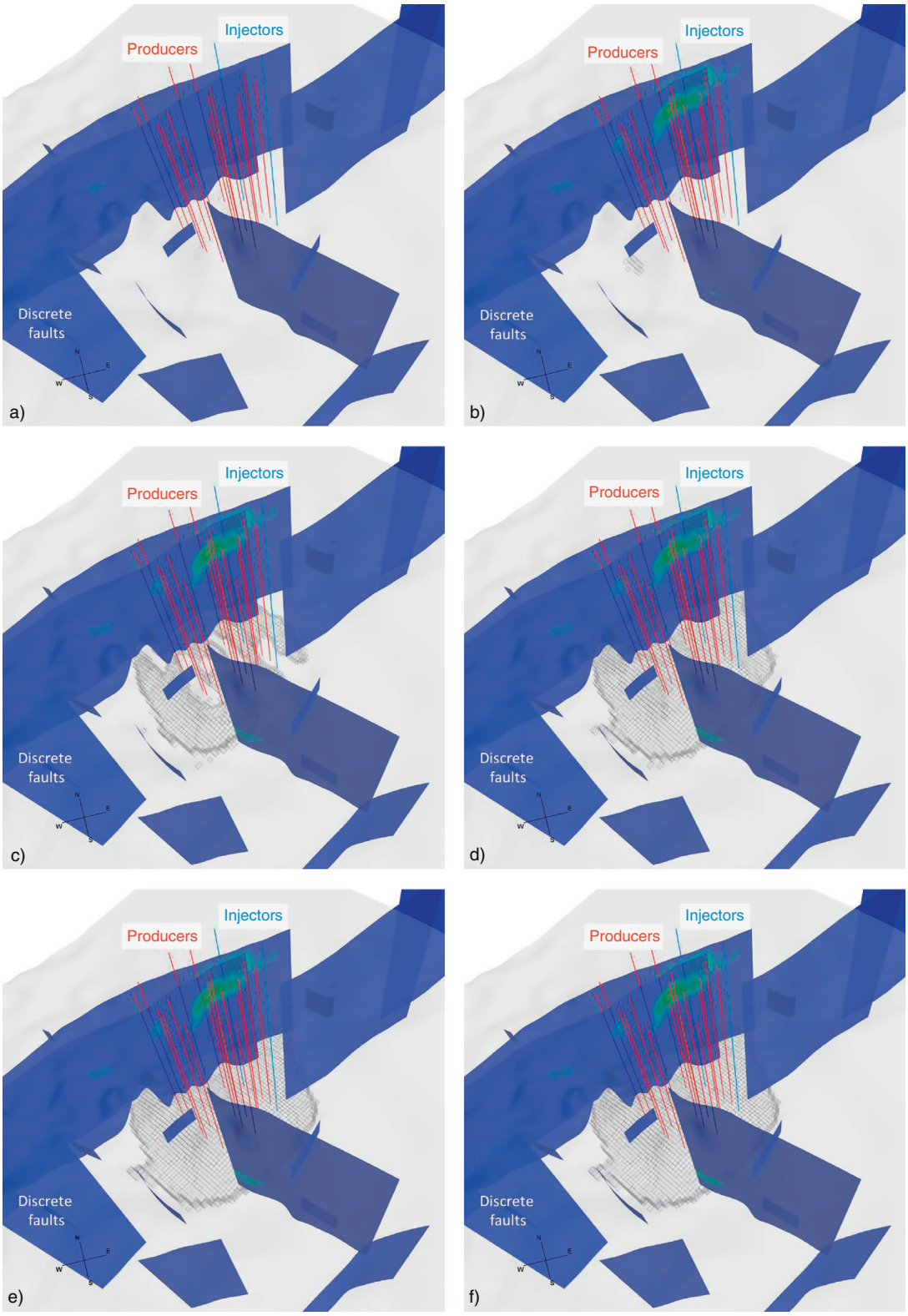

Figure 20

Fault shear failure (non-blue colours at fault planes) as well as plastification in the Ca1 reservoir, Saxonian aeolian and fluvial sandstones (transparent grid elements) in a) 1973 (initial state before gas production), b) 1981, c) 1991, d) 2001, e) 2012 (start of Co_2 injection) and f) 2153 (constant vertical displacements achieved). Transparent grey layer is the Ca1 reservoir top. Horizontal distance between the two injection wells (blue) is 1.6 km. Model exaggerated by a factor of 5.

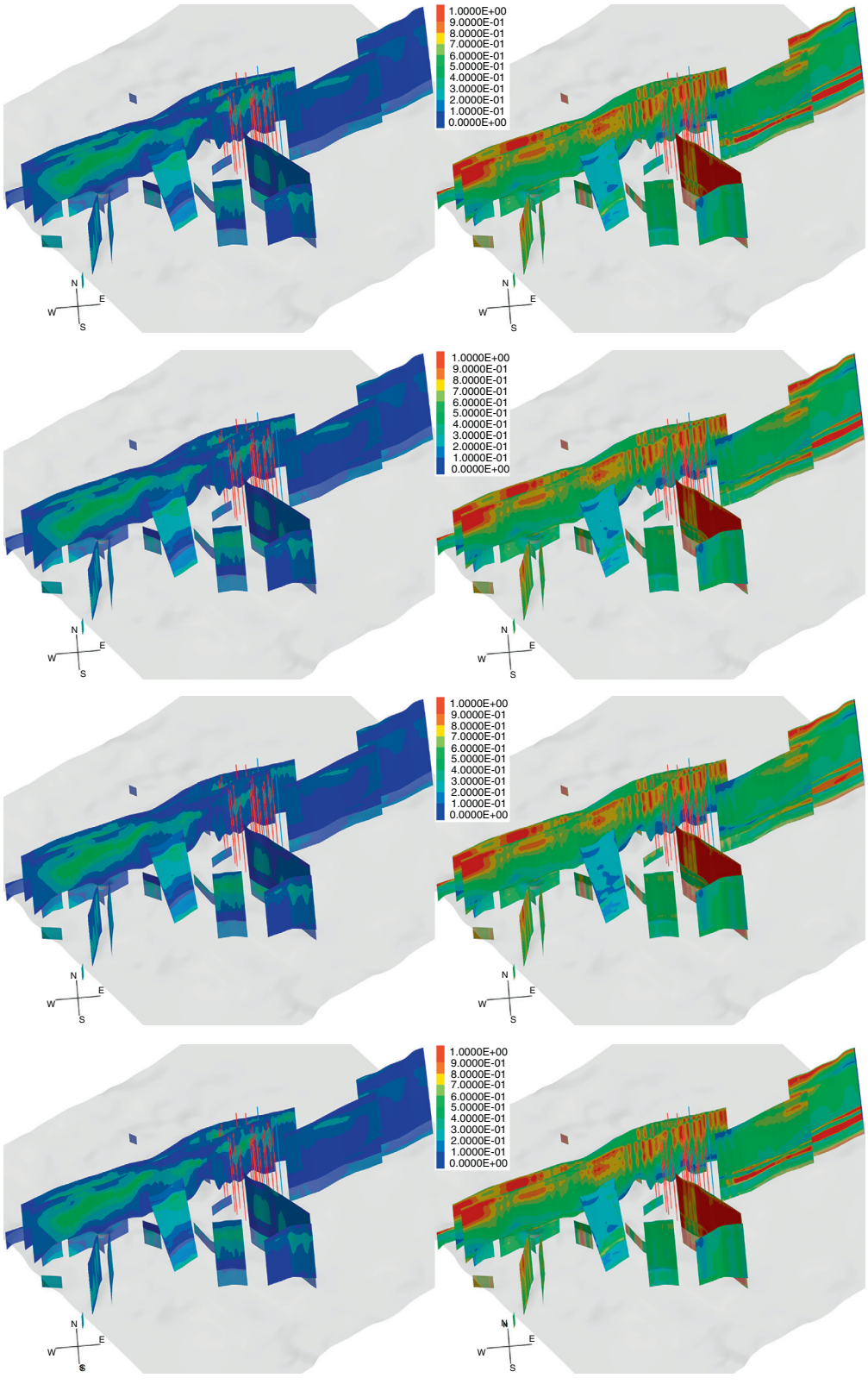

Figure 21

South view of fault slip (left) and dilation tendency (right) in 1973 (first row, before the start of gas production), 1981 (second row), 2012 (third row, start of CO_2 injection) and 2153 (fourth row, constant vertical displacements achieved). Grey shape indicates Ca1 Carbonate reservoir top. Vertical exaggeration by a factor of 5.

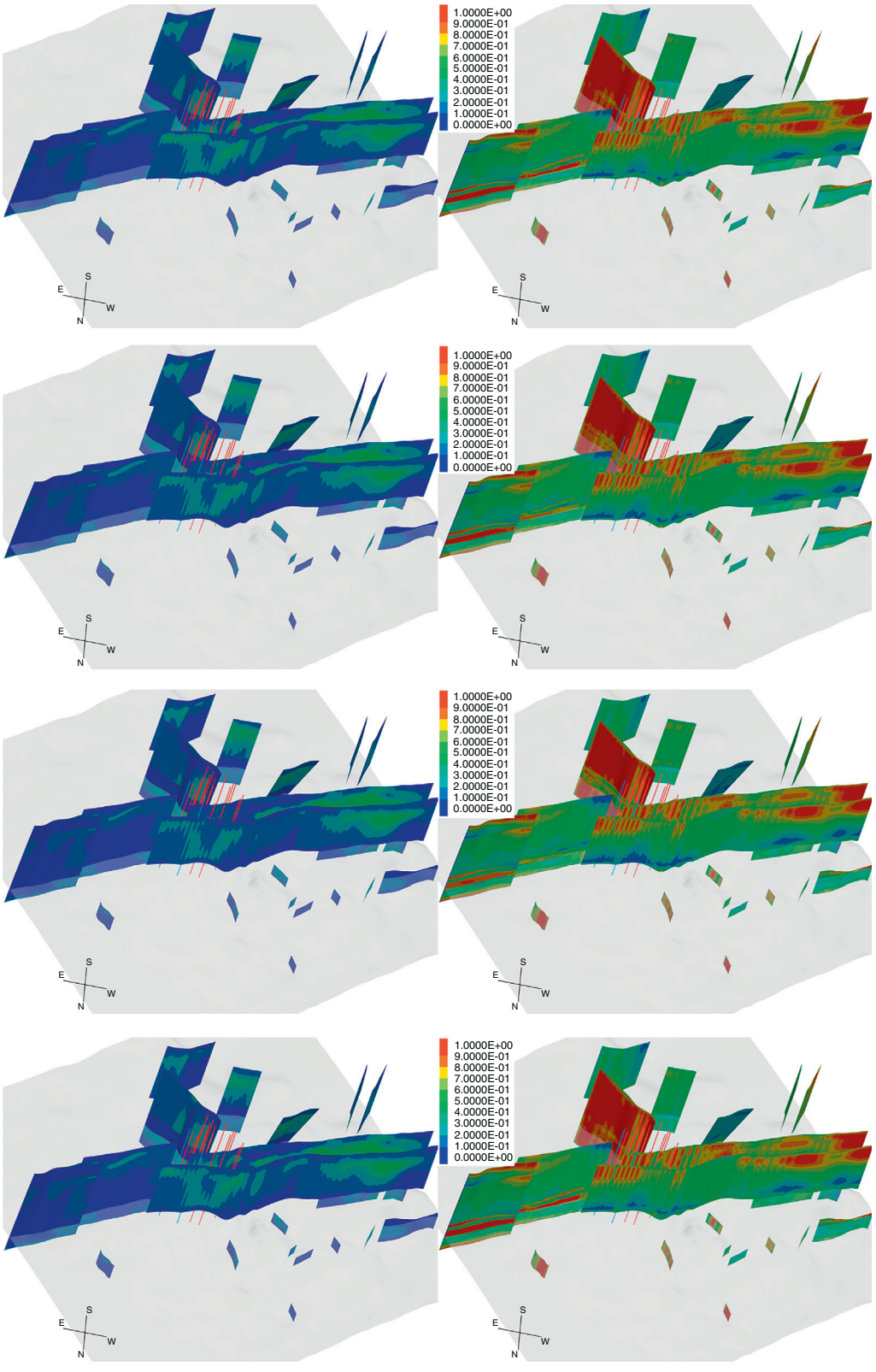

Figure 22

North view of fault slip (left) and dilation tendency (right) in 1973 (first row, before the start of gas production), 1981 (second row), 2012 (third row, start of CO_2 injection) and 2153 (fourth row, constant vertical displacements achieved). Grey shape indicates Ca1 Carbonate reservoir top. Vertical exaggeration by a factor of 5.

to exist or develop due to the excellent sealing capabilities of the Zechstein caprock units. Nevertheless, the numerical regional-scale model determined a fault reactivation at the depth level of the Upper Triassic at the two faults cutting the Załęcze gas field that should be further investigated by numerical modeling studies in advance of the start of the prospective EGR.

CONCLUSIONS

Production from the Załęcze natural gas field located in the Fore-Sudetic Monocline of the Southern Permian Basin has been carried out since late 1973. The initial pressure given with about 151 bar was reduced to 22 bar until 2011 as a result of continuous natural gas production. In the present study, we investigated a prospective EGR operation by a hypothetical CO_2 injection below the gas-water contact by application of coupled numerical simulations. For quantification of the CO_2 storage capacity and CO_2 trapping efficiency, two different injection scenarios were defined and assessed by means of dynamic flow simulations.

The two investigated scenarios are only distinguished by the length of the respective injection period; both scenarios consider an injection rate of 0.9 Mt CO_2/year. According to the regional industrial demands, the injection period duration is 20 years in the first scenario resulting in 17.78 Mt of CO_2 stored in the reservoir after that time; the average reservoir pressure is increased to 26% of the initial one. Since the injection well perforation is located below the gas-water contact, CO_2 trapping by dissolution as well as residual CO_2 trapping expose relatively high values at the end of the simulation (about 500 years), with a total trapping of 66.9% (11.9 Mt CO_2). The second simulation scenario was carried out to account for the maximum CO_2 storage capacity in the reservoir specifically limited by a maximum reservoir pressure of 151 bar not exceeding the initial one, which was reached after 118 years of CO_2 injection with a total calculated storage capacity of 106.6 Mt. Total CO_2 trapping is somewhat lower, with about 43% (45.8 Mt CO_2) after 500 years of simulation, since more than five times the amount of CO_2 is injected into the reservoir in the second scenario. Residual and solubility trapping are limited by the displacement of formation fluid in addition to a faster arrival at the maximum CO_2 saturation at the CO_2 brine interface. Consequently, the Załęcze natural gas field offers significant CO_2 storage capacity able to store CO_2 emissions form, *e.g.*, multiple lignite-fired power plants at a time-scale of a couple of decades.

Following the well measurement and dynamic flow simulations, two modeling groups carried out coupled hydro-mechanical simulations based on completely independent strategies of data integration and model implementation. A field-scale hydro-mechanical model including ten lithological units and two major faults was implemented to investigate the impact of applying a viscoelastic constitutive material law to the Zechstein seal by means of vertical displacements and potential fault reactivation. Here, due to the lack of dynamic flow simulation data at the time the simulations were carried out, the pore pressure was changed in the gas cap of the reservoir based on pressure monitoring point data from the production wells. Furthermore, a regional-scale hydro-mechanical model comprising twelve lithological units and 31 regional faults was elaborated using an elastoplastic constitutive law and aiming at a detailed assessment of fault slip and dilation tendency besides potential fault reactivation and vertical displacements. Deviations in the numerical simulation results between the two hydro-mechanical models can be explained by the chosen constitutive laws allowing for creep or plastification (irreversible deformation) or purely elastic behaviour of the lithological units only. Maximum displacements at minimum reservoir pressure were calculated to be 7.6 cm (pure elastic model), 11.2 cm (viscoelastic model for the Zechstein seal) and to 14.7 cm (elastoplastic model for all lithological units). Despite the constitutive laws applied, deviations arise from the fact that one model integrated the spatial pore pressure from the dynamic flow simulation, while the other one used point data from well measurements only. Nevertheless, both hydro-mechanical models indicate that only a low probability of fault reactivation exists, and furthermore, that a continuous leakage path for formation fluids or CO_2 is very unlikely to be present or to develop due to the excellent sealing properties of the Zechstein caprocks. Fault reactivation at reservoir depth was only achieved in the simulations where a partial reservoir repressurisation resulting from a laterally sealing fault was considered. However, this scenario is very unlikely, since laterally sealing faults have not been determined from the production data but only used in the dynamic flow simulations carried out in the present study to account for a potential mechanical limitation. In addition, our hydro-mechanical simulations emphasise the theory of independent supra- and subsaliniferous fault systems based on fault slip tendencies in the Zechstein salt and anhydrite units that are almost zero. The regional-scale model demonstrates that considering the given uniaxial compressive strength of the reservoir units, significant plastification (irreversible deformation) takes places in the reservoir units during the first three decades of the production period. Nevertheless, the seal integrity is not compromised, resulting from the initially low differential stresses in the Zechstein seal and its excellent sealing and self-healing capabilities.

Monitoring strategies accompanying CO_2 injection should consider the Ca2 reservoir as an indicator horizon for potential leakage of CO_2, natural gas and/or other Ca1

reservoir fluids. This would allow for observation of potential changes in the Ca2 reservoir pressure and fluid composition for early detection of a potential leakage from the Ca1 reservoir. Further, regular monitoring of operating as well as accessible wells penetrating the Ca1 reservoir, and thus also the primary caprock, should be taken into account to verify well integrity. Different state-of-the-art applications can be employed to determine cement and casing integrity as well as potential fluid migration along the cement-casing or cement-rock interfaces. Application of remote sensing (Interferometric Synthetic Aperture Radar - InSAR) may support detection of large-scale fault reactivation by monitoring differential displacements at the ground surface. This may be successfully accompanied by time-lapse seismics to observe the potential upward migration of fluids exhibiting a density contrast to the residual brine.

Since fault reactivation is occurring at two locations of the two east-striking faults, cutting the Załęcze reservoir units, at the depth of the Middle Triassic (Muschelkalk), further work should aim at a more detailed investigation of the impact of material and fault properties on fault behaviour at these depths. In particular, hydro-mechanical fault behaviour is a scientific question requiring further research by combining numerical modeling with field observations. Furthermore, a coupled hydro-mechanical simulation taking into account adjacent gas fields in production should be carried out to assess potential interaction of hydro-mechanical effects on a larger modeling scale.

Based on our coupled hydro-mechanical simulation results derived from two independent assessment strategies exhibiting similar findings on fault and caprock integrity, we conclude that the scheduled EGR scheme is feasible, with a negligibly low risk of relevant fault reactivation as well as highly unlikely formation fluid leakage through the Zechstein caprocks.

ACKNOWLEDGMENTS

The research leading to these results received funding from the European Union Seventh Framework Programme (FP7/2007-2013) under grant agreement No. 256705 (SiteChar project) as well as from *Enel*, *Gassnova*, *PGNiG*, *Statoil*, *Vattenfall*, *Veolia Environnement* and the Scottish Government. The authors are grateful for the efforts of the editor and two anonymous reviewers as well as of the anonymous proof-reader in increasing the manuscript quality.

REFERENCES

Bérest P., Blum P.A., Charpentier J.P., Gharbi H., Valès F. (2005) Very slow creep tests on rock samples, *Rock Mechanics and Mining Sciences* **42**, ARMA 14-7052.

Bérest P., Béraud J.F., Gharbi H., Brouard B., De Vries K. (2014) A very slow creep test on an Avery Island salt sample, *The 48th Rock Mechanics/Geomechanics Symposium*, Minneapolis, 1-4 June, ARMA 14-7052.

Cappa F., Rutqvist J. (2011) Modeling of coupled deformation and permeability evolution during fault reactivation induced by deep underground injection of CO_2, *International Journal of Greenhouse Gas Control* **5**, 2, 336-346.

CMG (2011) *GEM Advanced compositional and GHG reservoir simulator*, User's Guide.

Gou Y., Hou Z., Liu H., Zhou L., Were P. (2014) Numerical simulation of carbon dioxide injection for enhanced gas recovery (CO_2-EGR) in Altmark natural gas field, *Acta Geotechnica* **9**, 1, 49-58.

Hawkes C., McLellan P.J., Zimmer U., Bachu S. (2004) Geomechanical factors affecting geological storage of CO_2 in depleted oil and gas reservoirs: risks and mechanisms, *6th North American Rock Mechanics Symposium*, *Gulf Rocks 2004*, 5-9 June, Houston, paper No. 04-579.

Heidbach O., Tingay M., Barth A., Reinecker J., Kurfeβ D., Müller B. (2008) The World Stress Map database release 2008, doi: 10.1594/GFZ.WSM.Rel2008.

Hou Z., Gou Y., Taron J., Gorke U.J., Kolditz O. (2012) Thermo-hydro-mechanical modeling of carbon dioxide injection for enhanced gas-recovery (CO_2-EGR): A benchmarking study for code comparison, *Environmental Earth Sciences* **67**, 2, 549-561.

Hussen C., Amin R., Madden G., Evans B. (2012) Reservoir simulation for enhanced gas recovery: An economic evaluation, *Journal of Natural Gas Science and Engineering* **5**, 42-50.

Itasca (2013) FLAC3D – Fast Lagrangian Analysis of Continua in 3 Dimensions, User's Guide, First Revision (FLAC3D Version 5.01), Nov. 2013, Itasca Consulting Group Inc.

Jaeger J.C., Cook N.G.W., Zimmerman R.W. (2007) *Fundamentals of Rock Mechanics*, Fourth edition, Blackwell Publishing Ltd.

Jamaloei B.Y. (2013) A review of recent advances in the study of drainage in porous media, *Special Topics and Reviews in Porous Media* **4**, 3, 253-272.

Jarosinski M. (2005a) Ongoing tectonic reactivation of the Outer Carpathians and its impact on the foreland: Results of borehole breakout measurements in Poland, *Tectonophysics* **410**, 189-216.

Jarosinski M. (2005b) Recent tectonic stress regime in Poland based on analyses of hydraulic fracturing of borehole walls, *Przeglad Geologizny* **53**, 10/1, 863-872 (in Polish).

Jarzyna J., Puskarczyk E., Bała M., Papiernik B. (2009) Variability of the Rotliegend sandstones in the Polish part of the Southern Permian Basin - permeability and porosity relationships, *Annales Societatis Geologorum Poloniae* **79**, 13-26.

Karnkowski P.H. (1999) Origin and evolution of the Polish Rotliegend Basin, *PGI Special Papers* **3**, 1-93.

Karnkowski P.H. (2007) Permian Basin as a main exploration target in Poland, *Przegląd Geologiczny* **55**, 12/1, 1003-1015 (in Polish).

Kempka T., Nielsen C., Frykman P., Shi J.Q., Bacci G., Dalhoff F. (2015) Coupled Hydro-Mechanical Simulationsof CO_2 Storage Supported by Pressure Management Demonstrate Synergy Benefits from Simultaneous Formation Fluid Extraction, *Oil & Gas Science and Technology* **70**, 4, 599-613.

Kempka T., Klapperer S., Norden B. (2014) Coupled hydro-mechanical simulations demonstrate system integrity at the Ketzin pilot site for CO_2 storage, Germany. Rock Engineering and Rock Mechanics: Structures in and on Rock Masses, *Proceedings of EUROCK 2014, ISRM European Regional Symposium* 1317-1322.

Kühn M., Tesmer M., Pilz P., Meyer R., Reinicke K., Förster A., Kolditz O., Schäfer D. (2012) CLEAN: Project overview on CO_2 large-scale enhanced gas recovery in the Altmark natural gas field (Germany), *Environmental Earth Sciences* **67**, 2, 311-321.

Kühn M., Förster A., Großmann J., Lillie J., Pilz P., Reinicke K.M., Schäfer D., Tesmer M., CLEAN Partners (2013) The Altmark Natural Gas Field is prepared for the Enhanced Gas Recovery Pilot Test with CO_2, *Energy Procedia* **37**, 6777-6785.

Magoon L.B., Schmoker J.W. (2000) The total petroleum system – The natural fluid network that constrains the assessment unit, in U.S. Geological Survey World Petroleum Assessment 2000 – Description and results, USGS Digital Data Series DDS-60, Version 1.0, CD-ROM, Disk 1.

Magri F., Tillner E., Wang W., Watanabe N., Zimmermann G., Kempka T. (2013) 3D Hydro-mechanical Scenario Analysis to Evaluate Changes of the Recent Stress Field as a Result of Geological CO_2 Storage, *Energy Procedia* **40**, 375-383.

Nagelhout A.C.G., Roest J.P.A. (1997) Investigating fault slip in a model of an underground gas storage facility, *International Journal of Rock Mechanics & Mining Sciences* **34**, 3-4, Paper No. 212.

Nghiem L., Shrivastava V., Kohse B., Hassam M., Yang C. (2010) Simulation and optimization of trapping processes for CO_2 storage in saline aquifers, *Journal of Canadian Petroleum Technology* **49**, 8, 15-22.

Oldenburg C.M., Stevens S.H., Benson S.M. (2004) Economic feasibility of carbon sequestration with enhanced gas recovery (CSEGR), *Energy* **29**, 9-10, 1413-1422.

Orlic B., Wassing B.B.T. (2013) A study of stress change and fault slip in producing gas reservoirs overlain by elastic and visco-elastic caprocks, *Rock Mechanics and Rock Engineering* **46**, 421-435.

Orlic B., Mazurowski M., Papiernik B., Nagy S. (2013) Assessing the geomechanical effects of CO_2 injection in a depleted gas field in Poland by field scale modelling, *Proceedings of EUROCK 2013 - The 2013 ISRM International Symposium*, Kwaśniewski M., Łydżba D. (eds), Wrocław, 21-26 Sept., London, Taylor & Francis Group, pp. 969-975.

Ouellet A., Bérard T., Frykman P., Welsh P., Minton J., Pamucku Y., Hurter S., Schmidt-Hattenberger C. (2010) Reservoir geomechanics case study of seal integrity under CO2 storage conditions at Ketzin, Germany, Ninth Annual Conference on Carbon Capture and Sequestration, 10-13 May 2010.

Papiernik B., Buniak A., Hajto M., Kiersnowski H., Zych I., Machowski G., Jasnos J. (2008) Volumetric model of deposits of the Rotliegend and Zechstein Basal Limestone Ca1 based on core and petrophysical log interpretations, in *Prognostic resources and undiscovered gas potential of deposits of the Rotliegend and Zechstein Basal Limestone Ca1 in Poland*, Górecki W. (ed.), Polish Geol. Inst. Archive, Warsaw (in Polish).

Papiernik B., Kiersnowski H., Machowski G., Górecki W. (2012) Upper Rotliegend reservoir and facies models of geomorphological and structural gas traps in Silesian Basin - South-West Poland, *74th EAGE Conference and Exhibition*, 4-7 June, Copenhagen, P245.

Papiernik B., Doligez B., Klimkowski L. (2015) Structural and parametric models of the Załęcze and Żuchlów gas fields region, Fore-Sudetic Monocline, Poland - an example of general static modeling workflow in mature petroleum areas for CCS, EGR or EOR purposes, *Oil & Gas Science and Technology* **70**, 4, 635-654.

Pletsch T., Appel J., Botor D., Clayton C.J., Duin E.J.T., Faber E., Górecki W., Kombrink H., Kosakowski P., Kuper G., Kus J., Lutz R., Mathiesen A., Ostertag-Henning C., Papiernik B., van Bergen F. (2010) Petroleum Generation and Migration, in *Petroleum Geological Atlas of the Southern Permian Basin Area*, Doornenbal J.C., Stevenson A.G. (eds), EAGE Publications B.V., Houten.

Polak S., Grimstad A.A. (2009) Reservoir simulation study of CO_2 storage and CO_2-EGR in the Atzbach–Schwanenstadt gas field in Austria, *Energy Procedia* **1**, 1, 2961-2968.

Pruess K. (2011) Modeling CO_2 leakage scenarios, including transitions between super- and sub-critical conditions, and phase change between liquid and gaseous CO_2, *Energy Procedia* **4**, 3754-3761.

Röhmann L., Tillner E., Magri F., Kühn M., Kempka T. (2013) Fault Reactivation and Ground Surface Uplift Assessment at a Prospective German CO_2 Storage Site, *Energy Procedia* **40**, 437-446.

Rutqvist J. (2012) The geomechanics of CO_2 storage in deep sedimentary formations, *Geotechnical and Geological Engineering* **30**, 3, 525-551.

Schlumberger (2012) Petrel Seismic-To-Evaluation Software, Version 2011.1, Schlumberger Information Solutions.

Tillner E., Kempka T., Nakaten B., Kühn M. (2013) Brine migration through fault zones: 3D numerical simulations for a prospective CO_2 storage site in Northeast Germany, *International Journal of Greenhouse Gas Control* **19**, 689-703.

Tillner E., Shi J.-Q., Bacci G., Nielsen C.M., Frykman P., Dalhoff F., Kempka T. (2014) Coupled Dynamic Flow and Geomechanical Simulations for an Integrated Assessment of CO_2 Storage Impacts in a Saline Aquifer, *Energy Procedia* **63**, 2879-2893.

TNO Diana (2012) *DIANA: Finite element program and User Documentation*, version 9.4.4, (www.tnodiana.com).

van Heekeren H., Bakker T., Duquesnoy T., de Ruiter V., Mulder L. (2009) Abandonment of an extremely deep cavern at Frisia salt, *Proceedings of the SMRI Spring 2009 Technical Conference*, Krakow, Poland, pp. 30-42.

Vidal-Gilbert S., Nauroy J.F., Brosse E. (2009) 3D geomechanical modelling for CO_2 geologic storage in the Dogger carbonates of the Paris Basin, *International Journal of Greenhouse Gas Control* **3**, 3, 288-299.

Manuscript submitted in July 2014
Manuscript accepted in April 2015
Published online in August 2015

Cite this article as: Ł. Klimkowski, S. Nagy, B. Papiernik, B. Orlic and T. Kempka (2015). Numerical Simulations of Enhanced Gas Recovery at the Załęcze Gas Field in Poland Confirm High CO_2 Storage Capacity and Mechanical Integrity, *Oil Gas Sci. Technol* **70**, 4, 655-680.